Archive of Applied Mechanics 73 (2003) 1 – 25 © Springer-Verlag 2003
DOI 10.1007/s00419-002-0271-4

On 'best' shell models – From classical shells, degenerated and multi-layered concepts to 3D

W. B. Krätzig, D. Jun

Summary Problems of solid mechanics are most generally formulated within 3D continuum mechanics. However, engineering models favor reduced dimensions, in order to portray mechanical properties by surface or curvilinear approximations. Such attempts for dimensional reduction constitute interactions between theoretical formulations and numerical techniques. A classical reduced model for thin bodies is represented by shell theory, an approximation in terms of resultants and first-order moments. If the shell theory, with its inherent errors, is considered as qualitatively insufficient for a particular problem, a further improvement is given by solid shell models, which are gained by direct linear interpolation of the 3D kinematic relations. They improve considerably the analytic capabilities for shells, especially when their congenital locking effects are handled by variational 'convergence tricks'. The next step towards 3D quality are layered shells or solid shell elements. The present paper compares these three approximation stages from the point of view of multi-director (integral) transformations of classical continuum mechanics. It offers physical convergence requirements for each of the treated models.

Keywords Shell theory, Solid shell, Multi-layered shell, Multi-director continuum

1 Introduction

In engineering, shells or shell structures, generally, are curved bodies imbedded into the 3D Euclidean space $E3$. They are thin-walled, and their geometries obey the thinness hypothesis

$$\lambda = \max\left(\frac{h}{\min(R, L)}\right) \ll 1 \ , \tag{1}$$

in which h denotes the maximum shell thickness, min R the smallest radius of curvature, and min L the smallest structural dimension of the shell's middle surface F, which bisects the thickness at each point of the shell.

Shell structures are undoubtedly the most widely used structural components in modern technologies: pipes and tanks, chemical reactor containments, ship hulls, aircraft fuselages, space vehicles, balloons and bells are well-known examples. Roman cupolas, vaults of medieval cathedrals or domes of baroque churches form historical shell structures, as cooling towers, reinforced concrete shell roofs or membrane constructions do in modern civil engineering. And, finally, organic nature has developed during its evolution varieties of shell bodies like cell walls, plant leaves, shells of snails and mussels or blood vessels.

For technical investigation and numerical analysis of these shell structures, shell theories describe the load-carrying behavior and the deformation properties in the context of mechanics of solids. Remembering the thinness hypothesis (1), shell concepts form thinness approxi-

Received 3 April 2002; accepted for publication 13 November 2002

W. B. Krätzig (✉), D. Jun
Institute for Statics and Dynamics, Civil Engineering,
Ruhr-University Bochum, 44780 Bochum, Germany
e-mail: w.b.kraetzig@sd.ruhr-uni-bochum.de

Partial support to the present study by the German Science Foundation (DFG) within the Special Research Center (SFB) 398 is gratefully acknowledged.

mations of 3D continua, considering all mechanical effects in the thickness direction approximately up to linear terms, namely by zeroth- and first-order moments.

Linear approximations of the theory of 3D continua can be performed in two different ways. First, classical shell theories establish by means of differential geometry surface-like kinematics on F, introducing the first and second strain tensors $\alpha_{(\alpha\beta)}$, $\beta_{(\alpha\beta)}$ and the transverse shear measure γ_α. Then, they define energetically adjoint dynamic variables, namely the membrane force tensor $n^{(\alpha\beta)}$ as resultant in-plane stresses, their first moments assembled in the moment tensor $m^{(\alpha\beta)}$, and the shear force vector q^α as resultant stresses transverse to F. Further, the dynamic and kinematic differential field equations as well as the constitutive relations can be derived either heuristically, comp. e.g. [14, 19, 27], or with more mathematical rigor, as linear (first-order) approximations from 3D continuum mechanics, [51, 18, 29, 35].

Because of contradictory assumptions in these derivations, like plane-stress states for Kirchhoff-Love models, [27], supplemented by transverse shear for Reissner-Mindlin shell types, versus director inextensibility, the search for best possible first-order approximations became virulent, [14, 30]. This is true, especially, after the development of finite shell elements (FSE) renown for refined mathematical rigor, like adjointness of kinematic and equilibrium field operators or self-adjointness of the internal shell potential, [31]. Consistent (shear-deformable) shell theories formed in such a way possess five independent external kinematics at each point of the middle surface F, namely three displacements u_i and two rotations ω_α, see Fig. 1(a).

Thus, FSE with displacement interpolation contain linear thickness approximations for the in-plane displacements u_α, and a constant for the normal displacement u_3; they can be constructed free of locking phenomena. Their disadvantage clearly is the plane-stress assumption, which may cause severe constraints in the inelastic constitutive modeling.

Classical FSE reduce the mechanical response of a shell continuum to variables on F. This reduction represents a further disadvantage for these elements: in modern CAD concepts, primarily contours of bodies are modeled, in case of shells – the outer and inner surfaces. With such concepts in mind, the second alternative of forming shell models is to directly degenerate 3D continuum elements – at least over the shell thickness – by linear displacement interpolations to shell-like kinematics. Initially called degenerated shell concepts, [2, 41], now – after inclusion of the thickness stretch – these concepts are generally addressed as continuum-based 3D, [26], or just solid shell concepts, [20], and advantageously admit arbitrary 3D constitutive material models, see Fig. 1(b). Such FE have twice the number of nodal points of classical shell elements, with three displacements u_i as degrees of freedom (DOF), and, thus, yield a slightly increased deformability (thickness stretch).

The basic theory of 3D continuum mechanics, its variables, field equations, constitutive models and boundary conditions have been well understood since long. All details therein seem to be straightforward as compared to shell mechanics, with its variety of different theories, their complex equations, different approximation levels and unusual rotational DOFs. The difficulties of this concept result from linear displacement interpolations, because the thinness hypothesis (1) yields distinct element length scales, and stiffness matrices are weakly conditioned. Since the work [34], ever more stiffness deficiencies of these elements, known as locking phenomena, were discovered. They could be overcome by means of certain remedies [16, 48], which were sometimes rejected as 'useful tricks' or even as 'variational crimes'. After their origins became clearly understood, [45, 46, 47], this type of shell elements has rapidly developed towards a reliable simulation platform.

Locking phenomena are the consequence of lacking suitable deformability of the mechanical model, [3], which can be observed also in the history of numerical modeling of laminates. This

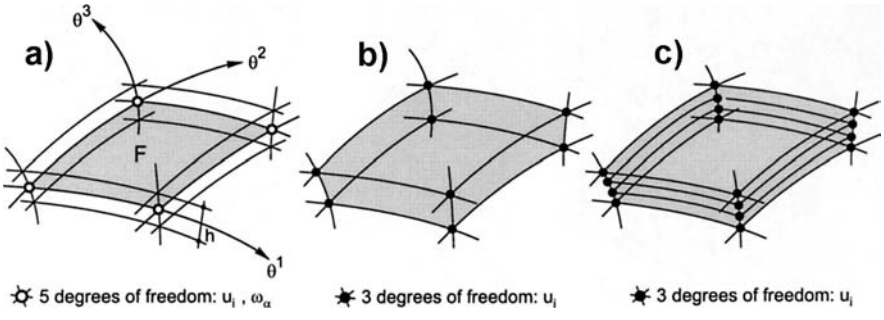

Fig. 1. Classical shell element **a**, solid shell element **b** and layered shell element with external refinement **c**

field improved with the development of more flexible, higher-order cross-sectional theories for shells with simple geometry, [37, 42]. Single-layered approaches possess at least C^1-continuity of the displacement fields across shell thickness, [38]. For multi-layered models, generally, C^0-continuity for the displacements of all layers over the thickness is considered as sufficient. This calls, at least, for Reissner-Mindlin-type shell theories as model constituents, [43] or, more advantageously from the viewpoint of geometry modeling, for solid shell elements [26], see Fig. 1(c). Both constituents should obey the thinness properties layer-wise

$$\lambda_N = \max\left(\frac{h_N}{\min(R, L)}\right) \ll 1 \ , \tag{2}$$

in which h_N denotes the single-layer thinness.

It has been discovered since long that compared to a single layer or a few layers with higher-order constituents, [40, 36], multi-layered models with low-order theories behave more advantageously. They are also more economical from the point of view of modern software for growing computer capabilities. This recognition is also due to aspects of model approximation capabilities, as Fig. 2 demonstrates, [5].

Multi-layered shell models represent a highly efficient concept in modern structural analysis. If the shell structure to be analyzed consists of composite laminate members, the application of layered finite shell elements is obvious. But even for transversely homogeneous structures, an inelastic response requires models with internal (layer-wise Gauss-point integration of inelastic constitutive laws) or even external (additional DOFs in layers) multi-layered refinement as the most advantageous and rigor analysis tools. If thickness discontinuities or local damage phenomena, like delamination or fiber cracking, are the aim of the investigation, only multi-layered element concepts provide the deformability necessary to avoid locking, which is inevitable for a correct phenomenon description.

The present paper intends to systematically explain the physical requirements for shell models, from classical to multi-layered theories, in dependence of the application aim. For sufficient physical generality, the treatment will be in tensor notation, applicable to arbitrary coordinates and geometry. All general statements will hold for small as well as for large shell displacements. Simplifications to beam models can easily be done.

2
Description of the multi-layered shell continuum

We start our treatment with some necessary preliminaries of geometry and kinematics. We consider an arbitrary shell continuum which later may consist of a suitable number of layers, packed densely upon each other, Fig. 3. The complete structure shall be imbedded into the 3D Euclidean space *E3*, the latter measurable by virtue of a right-handed orthogonal cartesian frame of reference x_i, e_i, $i = 1, 2, 3$. Material points P^* of the shell continuum shall be fixed by the curvilinear, convective coordinate system

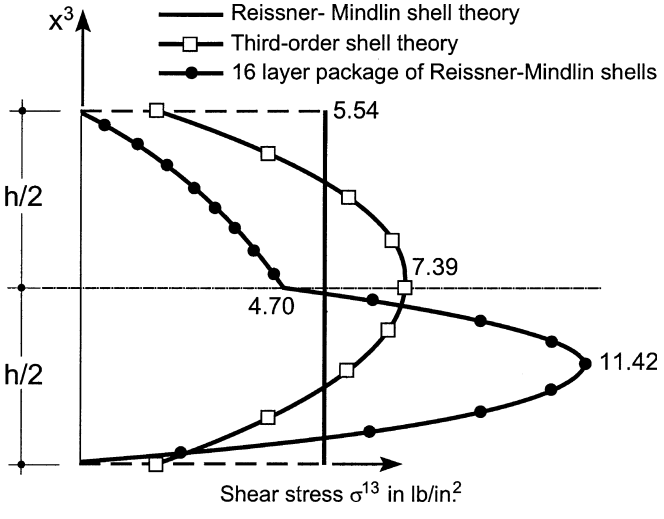

Fig. 2. Transverse shear stress $\sigma_{<13>}$ of asymmetric twofold cross-ply laminate by different theories [5]

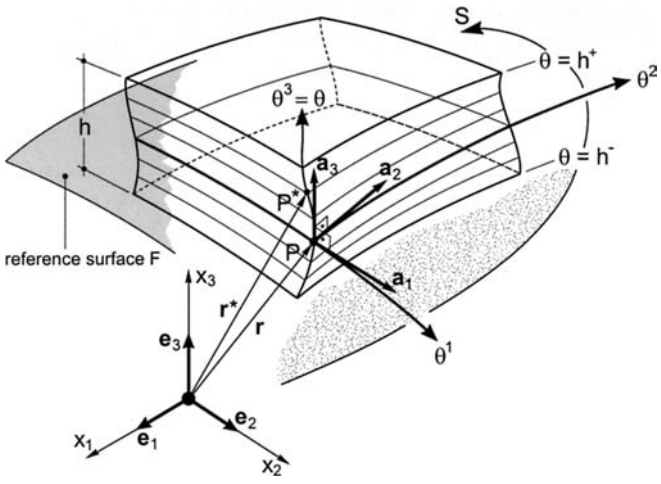

Fig. 3. Element of multi-layered shell continuum in its actual state

$$\theta^i, i = 1,2,3 : \theta^1, \theta^2, \theta^3 = \theta, \quad \frac{\mathrm{D}\theta^i}{\mathrm{D}t} = \dot{\theta^i} = 0 \ . \tag{3}$$

For all times t, the transformation between x_i and θ^i shall be inversely unique. The specification $\theta^3 = \theta = 0$ defines the reference (middle) surface F of the shell continuum, Fig. 3.

The position vector $\mathbf{r}^*$ of a generic point P^* outside of F of the actual configuration shall be represented by the following vector polynomial:

$$\mathbf{r}^* = \mathbf{r}^*(\theta^\alpha, \theta, t) = \sum_{n=0,1}^{\infty} \theta^n \mathbf{d}_n(\theta^\alpha, t), \alpha = 1,2 \ , \tag{4}$$

with θ^n as the nth polynomial term of θ^3, namely $\theta^n = (\theta^3)^n$. Herein

$$\mathbf{d}_n = \mathbf{d}_n(\theta^\alpha, t), n = 0,1,\ldots,\infty \ , \tag{5}$$

denotes an infinite set of vectors on F, classically named directors, [17]. Consequently, multi-layered packages described by (4) shall be later addressed as multi-layer, multi-director continua. Specification of $\theta = 0$ in (4)

$$\mathbf{r} = \mathbf{r}(\theta^\alpha, \theta = 0, t) = \mathbf{d}_0(\theta^\alpha, t) \ , \tag{6}$$

establishes the position vector $\mathbf{r}$ of the reference surface F, on which the shell boundary $s = s(\theta^\alpha, t)$ as a simply connected curve separates the interior shell domain from its exterior. As shown in Fig. 3, both bounding surfaces $\theta = h^+$ and $\theta = h^-$ act as faces of the considered shell, such that the shell body B is defined as $B = \{\theta^\alpha, \theta^3 : \theta^\alpha \in s, \theta^3 = \theta \in [h^+, h^-]\}$ with the shell domain s on the mid-surface.

In correspondence to (4), the velocity vector field $\mathbf{v}^*$ of material points P^* of the multi-director continuum is established by the material time derivative of the position vector $\mathbf{r}^*$ as

$$\mathbf{v}^* = \mathbf{v}^*(\theta^\alpha, \theta, t) = \frac{\mathrm{D}}{\mathrm{D}t}\mathbf{r}^* = \dot{\mathbf{r}}^* = \sum_{n=0,1}^{\infty} \theta^n \dot{\mathbf{d}}_n(\theta^\alpha, t) = \sum_{n=0,1}^{\infty} \theta^n \mathbf{v}_n(\theta^\alpha, t) \tag{7}$$

with $\mathbf{v}_n = \dot{\mathbf{d}}_n$.

We recall that the velocity field classically is introduced as time derivative of the displacement vector field $\mathbf{u}^*$

$$\mathbf{v}^* = \frac{\mathrm{D}}{\mathrm{D}t}\mathbf{u}^* \ , \tag{8}$$

the latter being defined by the difference of the position vectors of the actual state at time t and the undeformed state at $\overset{0}{t}$

$$\mathbf{u}^* = \mathbf{u}^*(\theta^\alpha, \theta, t) = \mathbf{r}^*(\theta^\alpha, \theta, t) - \overset{0}{\mathbf{r}}{}^*(\theta^\alpha, \theta, t = \overset{0}{t}) = \sum_{n=0,1}^{\infty} \theta^n (\mathbf{d}_n - \overset{0}{\mathbf{d}}_n) = \sum_{n=0,1}^{\infty} \theta^n \mathbf{u}_n \ . \tag{9}$$

By comparison of (8) and (9), we find $\mathbf{v}_n = \dot{\mathbf{u}}_n = \dot{\mathbf{d}}_n$.

All future physical considerations in connection with the shell continuum shall be described on the basis of its reference surface F, Eq. (6), in the actual state. In order to introduce on it elements of differential geometry, we establish a set of vectors $\mathbf{a}_\alpha$ by partial derivative of $\mathbf{r}$ with respect to θ^α as well as a unit normal vector $\mathbf{a}_3$

$$\mathbf{a}_\alpha = \frac{\partial}{\partial \theta^\alpha}\mathbf{r} = \mathbf{r}_{,\alpha} = \mathbf{d}_{0,\alpha}, \quad \mathbf{a}_3 = \mathbf{a}^3 = \frac{\mathbf{a}_1 \times \mathbf{a}_2}{|\mathbf{a}_1 \times \mathbf{a}_2|} \ . \tag{10}$$

This local covariant base $\mathbf{a}_\alpha, \mathbf{a}_3$ admits the installation of all necessary geometrical elements ($\mathbf{a}^\alpha, \mathbf{a}^3$-contravariant base, $a_{\alpha\beta}, a^{\alpha\beta}$-metric tensors, δ^α_β-Kronecker delta) with its corresponding relations

$$\mathbf{a}_\alpha = a_{\alpha\beta}\mathbf{a}^\beta, \quad \mathbf{a}^\alpha = a^{\alpha\beta}\mathbf{a}_\beta, \quad \mathbf{a}_\alpha \cdot \mathbf{a}^\beta = \delta^\beta_\alpha \ , \tag{11}$$

$$a_{\alpha\beta} = \mathbf{a}_\alpha \cdot \mathbf{a}_\beta, \quad a^{\alpha\beta} = \mathbf{a}^\alpha \cdot \mathbf{a}^\beta, \quad a_{\alpha\beta}a^{\beta\lambda} = \delta^\lambda_\alpha, \quad a = \det\, a_{\alpha\beta} \ , \tag{12}$$

$$\mathbf{a}_3 \cdot \mathbf{a}_3 = 1, \quad \mathbf{a}_\alpha \cdot \mathbf{a}_3 = 0, \quad \mathbf{a}_{3,\alpha} \cdot \mathbf{a}_3 = 0 \ . \tag{13}$$

These formulae shall be supplemented by the definitions of the curvature tensor $b_{\alpha\beta}$ of F and of the permutation tensor $\varepsilon_{\alpha\beta}$

$$b_{\alpha\beta} = -\mathbf{a}_\alpha \cdot \mathbf{a}_{3,\beta} = -\mathbf{a}_\beta \cdot \mathbf{a}_{3,\alpha} = \mathbf{a}_3 \cdot \mathbf{a}_{\alpha,\beta} = \mathbf{a}_3 \cdot \mathbf{a}_{\beta,\alpha} \ , \tag{14}$$

$$\begin{aligned} &\mathbf{a}_\alpha \times \mathbf{a}_\beta = \varepsilon_{\alpha\beta}\mathbf{a}^3, \quad \mathbf{a}^\alpha \times \mathbf{a}^\beta = \varepsilon^{\alpha\beta}\mathbf{a}_3 \ , \\ &\mathbf{a}_3 \times \mathbf{a}_\beta = \varepsilon_{\beta\lambda}\mathbf{a}^\lambda, \quad \mathbf{a}^3 \times \mathbf{a}^\beta = \varepsilon^{\beta\lambda}\mathbf{a}_\lambda \ , \end{aligned} \tag{15}$$

with the following properties

$$\varepsilon_{12} = -\varepsilon_{21} = \sqrt{a}, \quad \varepsilon^{12} = -\varepsilon^{21} = 1/\sqrt{a}, \quad \varepsilon_{11} = \varepsilon_{22} = \varepsilon^{11} = \varepsilon^{22} = 0 \ . \tag{16}$$

We further add the Weingarten formulae, which describe the covariant derivatives of the base vectors, [7, 19],

$$\mathbf{a}_{\alpha,\beta} = \Gamma^\lambda_{\alpha\beta}\mathbf{a}_\lambda + b_{\alpha\beta}\mathbf{a}_3, \ \mathbf{a}^\alpha_{,\beta} = -\Gamma^\alpha_{\beta\lambda}\mathbf{a}^\lambda + b^\alpha_\beta\mathbf{a}_3, \ \mathbf{a}_{3,\alpha} = -b^\lambda_\alpha\mathbf{a}_\lambda = -b_{\alpha\lambda}\mathbf{a}^\lambda \ . \tag{17}$$

As the reference surface F deforms with time t, all geometrical elements of F are functions of t. Since material time derivatives and partial derivatives are interchangeable, we gain under consideration of (10) the following connection for the time derivative of the covariant base vectors of F:

$$\mathbf{v}_{,\alpha} = \mathbf{v}_{0,\alpha} = \frac{\mathrm{D}}{\mathrm{D}t}\mathbf{r}_{,\alpha} = \frac{\mathrm{D}}{\mathrm{D}t}\mathbf{d}_{0,\alpha} = \frac{\mathrm{D}}{\mathrm{D}t}\mathbf{a}_\alpha = \dot{\mathbf{a}}_\alpha \ . \tag{18}$$

From there, after decomposition of the velocity $\mathbf{v}_0$ with respect to the base $\mathbf{a}^i$

$$\mathbf{v}_0 = v_{0\beta}\mathbf{a}^\beta + v_{03}\mathbf{a}^3 \ , \tag{19}$$

follows the expression

$$\dot{\mathbf{a}}_\alpha = \mathbf{v}_{0,\alpha} = \left(v_{0\beta}|_\alpha - v_{03}b_{\alpha\beta}\right)\mathbf{a}^\beta + \left(v_{03,\alpha} + v_{0\lambda}b^\lambda_\alpha\right)\mathbf{a}^3 = \varphi_{\beta\alpha}\mathbf{a}^\beta + \varphi_{3\alpha}\mathbf{a}^3 \ , \tag{20}$$

in which bars denote covariant derivatives on F. Combining (20) with the time derivative of (13), the complete base transformation reads

$\dot{\mathbf{a}}_i = \varphi_{ki}\mathbf{a}^k$:

$$\varphi_{ki} = \mathbf{a}_k \cdot \dot{\mathbf{a}}_i = \begin{bmatrix} \varphi_{\beta\alpha} & \varphi_{\beta 3} \\ \varphi_{3\alpha} & \varphi_{33} \end{bmatrix} = \begin{bmatrix} v_{0\beta}|_\alpha - v_{03} b_{\alpha\beta} & -\left(v_{03,\beta} + v_{0\lambda} b^\lambda_\beta\right) \\ v_{03,\alpha} + v_{0\lambda} b^\lambda_\alpha & 0 \end{bmatrix} \ . \tag{21}$$

Composing the time derivative of (12), we find the alternative form for the contravariant base vectors

$\dot{\mathbf{a}}^i = -\varphi^{ik}\mathbf{a}_k$:

$$\varphi^{ik} = -\dot{\mathbf{a}}^i \cdot \mathbf{a}_k = \begin{bmatrix} \varphi^{\alpha\beta} & \varphi^{\alpha 3} \\ \varphi^{3\beta} & \varphi^{33} \end{bmatrix} = \begin{bmatrix} v_0^\alpha|^\beta - v_{03} b^{\alpha\beta} & -\left(v^\beta_{03,} + v^\lambda_0 b^\beta_\lambda\right) \\ v^\beta_{03,} + v^\lambda_0 b^\beta_\lambda & 0 \end{bmatrix} \ . \tag{22}$$

Both definitions of the velocity gradients $\varphi_{ki}, \varphi^{ik}$ set the starting point for derivation of the kinematics of the shell continuum. For completeness, the above terms shall be supplemented by time derivatives of the metric as well as the permutation tensor

$$\dot{a}_{\alpha\beta} = 2\varphi_{(\alpha\beta)}, \quad \dot{a}^{\alpha\beta} = -a^{\alpha\lambda}a^{\beta\varrho}\dot{a}_{\lambda\varrho} = -2\varphi^{(\alpha\beta)} \ , \tag{23}$$

$$\dot{\varepsilon}_{\alpha\beta} = \dot{\sqrt{a}} = \varphi^\lambda_\lambda \varepsilon_{\alpha\beta} = \varphi^\lambda_\lambda \sqrt{a} \ . \tag{24}$$

From these fundamentals, we are already able to derive the time derivatives of the first and second strain tensors, [7, 19], of the reference surface F

$$\alpha_{(\alpha\beta)} = \frac{1}{2}\left(a_{\alpha\beta} - \overset{0}{a}_{\alpha\beta}\right), \quad \omega_{(\alpha\beta)} = -\left(b_{\alpha\beta} - \overset{0}{b}_{\alpha\beta}\right) \ , \tag{25}$$

namely

$$\dot{\alpha}_{(\alpha\beta)} = \frac{1}{2}\dot{a}_{\alpha\beta} = \varphi_{(\alpha\beta)} = \frac{1}{2}\left(\varphi_{\alpha\beta} + \varphi_{\beta\alpha}\right) = \frac{1}{2}\left(v_{0\alpha}|_\beta + v_{0\beta}|_\alpha - 2v_{03}b_{\alpha\beta}\right) \ , \tag{26}$$

$$\begin{aligned} \dot{\omega}_{(\alpha\beta)} &= -\dot{b}_{\alpha\beta} = -\frac{1}{2}\left(\varphi_{3\alpha}|_\beta + \varphi_{3\beta}|_\alpha + \varphi_{\lambda\alpha}b^\lambda_\beta + \varphi_{\lambda\beta}b^\lambda_\alpha\right) \\ &= \frac{1}{2}\left(v_{03}|_{\alpha\beta} + v_{03}|_{\beta\alpha} + 2v_{0\lambda}|_\alpha b^\lambda_\beta + 2v_{0\lambda}|_\beta b^\lambda_\alpha + v_{0\lambda}\left(b^\lambda_\alpha|_\beta + b^\lambda_\beta|_\alpha\right) - 2v_{03}b_{\alpha\lambda}b^\lambda_\beta\right) \ . \end{aligned} \tag{27}$$

3
The applied concept in 3D description

In this investigation, requirements for shell models shall be derived. However, in this Section, we will briefly sketch the applied concept in the classical 3D description. We start with the global statement of energy conservation as a rate-of-work equation for isothermal processes, written in 3D form, [49, 35],

$$\frac{\mathrm{D}}{\mathrm{D}t}\int_V \left(U^* + \frac{1}{2}\mathbf{v}^* \cdot \mathbf{v}^*\right)\varrho^* \mathrm{d}V - \int_V \mathbf{f}^* \cdot \mathbf{v}^* \varrho^* \mathrm{d}V - \int_S \mathbf{t}^* \cdot \mathbf{v}^* \mathrm{d}S = 0 \ , \tag{28}$$

which contains only mechanical state variables of the continuum at time t. Therein, all functions of the three convective curvilinear coordinates θ^i, s. Fig. 3, are marked by a star. Equation (28) contains the following symbols: $\mathrm{d}V = \sqrt{g}\mathrm{d}\theta^1\mathrm{d}\theta^2\mathrm{d}\theta^3$ denotes the material volume element of the shell continuum with $g = \det g_{ij}$ as the determinant of the 3D metric tensor, $\mathrm{d}S$ is a free surface element of the body, U^* denotes the internal energy density related to the mass density ϱ^*, $\mathbf{f}^*$ is the field of body forces per unit mass, and $\mathbf{t}^*$ is the field of tractions on $\mathrm{d}S$; $\mathbf{v}^* = \dot{\mathbf{u}}^*$ represents the velocity field.

If we continue the 3D treatment, we proceed as follows: introduce the Cauchy stress tensor σ^{ij}, [8, 9] into (28) by

$$\mathbf{t}^* = \frac{n_i \mathbf{T}^{*i}}{\sqrt{g}} = \sigma^{ij} n_i \mathbf{g}_j, \quad \mathbf{T}^{*i} = \sqrt{g}\sigma^{ij}\mathbf{g}_j, \quad \mathbf{n} = n_i \mathbf{g}^i \ , \tag{29}$$

and transform the surface integral in (28) by the use of the Green-Gauss theorem

$$\int_S n_i b^i \mathrm{d}S = \int_V \frac{1}{\sqrt{g}} \left(\sqrt{g} b^i\right)_{,i} \mathrm{d}V \ . \tag{30}$$

A localization procedure of the volume integral furnishes the local form of the rate-of-energy equation (28). Invariance requirements of this local statement of energy conservation under superposed infinitesimal rigid body translations and rotations, [49, 18], yield the equations of motion

$$\mathbf{T}^{*i}_{,i} + \varrho^* \sqrt{g}(\mathbf{f}^* - \dot{\mathbf{v}}^*) = 0 : \sigma^{ij}|_i + \varrho \bar{f}^{*j} = 0 \text{ with } \bar{f}^{*j} = f^{*j} - \dot{v}^{*j} \ , \tag{31}$$

and the symmetry condition

$$\mathbf{T}^{*i} \times \mathbf{g}_i = 0 : \sigma^{ij} = \sigma^{ji} \ . \tag{32}$$

There remains the internal energy statement

$$-\varrho^* \dot{U}^* + \frac{1}{2}\sigma^{ij}\dot{g}_{ij} = 0 \ , \tag{33}$$

if conservation of mass is observed

$$\frac{\mathrm{D}}{\mathrm{D}t}\varrho^* \sqrt{g} = 0 : \dot{\varrho}^* + v^i|_i \varrho^* = 0 \ . \tag{34}$$

We now assume the internal energy U^* to be solely a function of the Green-Lagrange strain tensor γ_{ij}, $U^* = U^*(\gamma_{ij})$. Its time-derivative equals half the rate of the metric tensor

$$\gamma_{ij} = \frac{1}{2}\left(g_{ij} - \overset{0}{g}_{ij}\right), \quad \dot{g}_{ij} = 2\dot{\gamma}_{ij} \ . \tag{35}$$

The following transformation in (33):

$$-\varrho^* \dot{U}^* = -\varrho^* \frac{\partial U^*}{\partial t} = -\varrho^* \frac{\partial U^*}{\partial \gamma_{ij}} \frac{\partial \gamma_{ij}}{\partial t} = -\varrho^* \frac{\partial U^*}{\partial \gamma_{ij}} \dot{\gamma}_{ij} \ , \tag{36}$$

yields

$$\sigma^{ij} = \varrho^* \frac{\partial U^*}{\partial \gamma_{ij}} \ , \tag{37}$$

i.e. the constitutive law of hyperelasticity for the Cauchy stress tensor. Finally, we add the kinematic definition of the Green-Lagrange strain tensor, [19], e.g. in linearized version

$$\gamma_{ij} = \frac{1}{2}(u_i|_j + u_j|_i) \qquad \text{from} \qquad \dot{\gamma}_{ij} = \frac{1}{2}(v_i|_j + v_j|_i) \ . \tag{38}$$

Thus, all interior physical equations have been established: the kinematic (38) and dynamic (31, 32) field conditions and the constitutive statement (37). This very procedure shall now be repeated after semi-discretization of the shell continuum in the θ^3-thickness direction.

4
Semi-discretization into a multi-director continuum

We return to the statement (28) of energy conservation, as applied now to our shell continuum, Fig. 3. Presently, no assumptions on its cross-sectional physical structure or mechanical

modeling have been made. The intended semi-discretization in the θ^3-direction has been advantageously predisposed by developing the position vector $\mathbf{r}^*$, Eq. (4), and the velocity vector $\mathbf{v}^*$, Eq. (7), into polynomial series expansions in θ^n, $n = 0, 1, \ldots, \infty$. We generalize the integrand of (28), after having transformed the surface integral into a volume one according to (30), and introduce in last a time-independent scalar trial function

$$\phi = \phi(\theta^1, \theta^2, \theta^3), \quad \dot{\phi} = 0 \ . \tag{39}$$

Retransformation of

$$\int_V \frac{1}{\sqrt{g}} \left\{ [\mathbf{T}^{*i} \cdot \mathbf{v}^*] \phi \right\}_{,i} \mathrm{d}V$$

into a surface integral again by virtue of (30), yields the following generalized energy statement:

$$\frac{\mathrm{D}}{\mathrm{D}t} \int_V \left(U^* + \frac{1}{2} \mathbf{v}^* \cdot \mathbf{v}^* \right) \varrho^* \phi \, \mathrm{d}V - \int_V \mathbf{f}^* \cdot \mathbf{v}^* \varrho^* \phi \, \mathrm{d}V - \int_S \mathbf{t}^* \cdot \mathbf{v}^* \phi \, \mathrm{d}S + \int_V \frac{1}{\sqrt{g}} \mathbf{T}^{*i} \cdot \mathbf{v}^* \phi_{,i} \, \mathrm{d}V = 0 \ , \tag{40}$$

which will be the basis of our future derivations. We can specify now the trial function (39) as an arbitrary term of the polynomial function space

$$\phi = \theta^l, \qquad l = 0, 1, \ldots, \infty \tag{41}$$

and introduce additionally definitions (4, 7). Thus, we are able to execute the semi-discretization in all integrals of Eq. (40). For example, regarding (7) the first integral in (40) will be transformed into

$$\frac{\mathrm{D}}{\mathrm{D}t} \int_V \left(U^* + \frac{1}{2} \mathbf{v}^* \cdot \mathbf{v}^* \right) \varrho^* \theta^l \, \mathrm{d}V = \frac{\mathrm{D}}{\mathrm{D}t} \int_F \int \varrho \left(U^l + \frac{1}{2} \sum_{m,n=0,1}^{\infty} k^{l+m+n} \mathbf{v}_m \cdot \mathbf{v}_n \right) \sqrt{a} \ \mathrm{d}\theta^1 \ \mathrm{d}\theta^2 \ , \tag{42}$$

in which the sets of moments U^l of integral transforms of the internal energy density are defined by the through-thickness integrals

$$\varrho U^l \sqrt{a} = \int_{h^-}^{h^+} U^* \varrho^* \theta^l \sqrt{g} \ \mathrm{d}\theta, \quad l = 0, 1, \ldots, \infty \ , \tag{43}$$

and those of the moments ϱk^l of the mass density by

$$\varrho k^l \sqrt{a} = \int_{h^-}^{h^+} \varrho^* \theta^l \sqrt{g} \mathrm{d}\theta, \quad l = 0, 1, \ldots, \infty \ . \tag{44}$$

The symbol k^{l+m+n} in (42) is formed by substitution of $\theta^l \cdot \theta^m \cdot \theta^n$ in (44). We discover that this semi-discretization process, due to the special choice of ϕ in (41), – furnishes an expression of the rate-of-energy equation, which is based on the reference surface F. For instance, Eq. (44) delivers for $l = 0 \Rightarrow k^0 = 1$

$$\varrho k^0 \sqrt{a} = \int_{h^-}^{h^+} \varrho^* \sqrt{g} \ \mathrm{d}\theta \tag{45}$$

the resulting mass density of the shell as its zeroth moment.

For further details of this semi-discretization process we refer to [32], for refined information to [29] and [35]. Considering relations (29, 30) in the corresponding terms of (40), we find the semi-discretized form of the generalized rate-of-energy equation as

$$\frac{\mathrm{D}}{\mathrm{D}t}\iint\limits_F \varrho\left(U^l+\frac{1}{2}\sum_{m,n=0,1}^{\infty} k^{l+m+n}\mathbf{v}_m\cdot\mathbf{v}_n\right)\,\mathrm{d}F+\iint\limits_F\sum_{n=0,1}^{\infty}\left(l\mathbf{m}^{l+n}-\varrho p^{l+n}\right)\mathbf{v}_n\,\mathrm{d}F$$
$$-\oint\limits_s\sum_{n=0,1}^{\infty}\mathbf{m}^{l+n\,\alpha}\cdot\mathbf{v}_n u_\alpha \mathrm{d}s=0\ . \tag{46}$$

Herein, the following sets of integral transforms complete the previous ones, Eqs. (43, 44):

– the moments ϱp^l of the body forces and tractions on the shell faces h^+, h^-

$$\varrho p^l\sqrt{a}=\int\limits_{h^-}^{h^+}\mathbf{f}^*\varrho^*\theta^l\sqrt{g}\,\mathrm{d}\theta+\left[\mathbf{t}^*\theta^l\sqrt{gg^{33}}\right]_{h^-}^{h^+},\quad l=0,1,\ldots,\infty\ , \tag{47}$$

– the moments $\mathbf{m}^{l\alpha}$ of the internal stresses $\mathbf{T}^{*\alpha}$, directed parallel to F

$$\mathbf{m}^{l\alpha}\sqrt{a}=\int\limits_{h^-}^{h^+}\mathbf{T}^{*\alpha}\theta^l\,\mathrm{d}\theta,\quad l=0,1,\ldots,\infty\ , \tag{48}$$

– the moments $\mathbf{m}^l$ of the internal stresses $\mathbf{T}^{*3}$, directed transversely to F

$$\mathbf{m}^l\sqrt{a}=\int\limits_{h^-}^{h^+}\mathbf{T}^{*3}\theta^{l-1}\,\mathrm{d}\theta,\quad l=0,1,\ldots,\infty\ . \tag{49}$$

In Eq. (46), the surface elements $\mathrm{d}F$ and line elements $\mathrm{d}s$ of the shell boundary s read, [7, 19],

$$\mathrm{d}F=\sqrt{a}\,\mathrm{d}\theta^1\,\mathrm{d}\theta^2,\quad u_\alpha\,\mathrm{d}s=\varepsilon_{\alpha\beta}\,\mathrm{d}\theta^\beta\ . \tag{50}$$

At this point, we have concluded the semi-discretization in the θ^3-direction and are thus able to repeat all steps of Sect. 3. We localize the semi-discretized set of energy statements (46) by executing the time derivative of the first integral, then transforming the last line integral into a surface one, [7, 19], and finally deleting the integral sign in front of the united energy term by requiring continuity of the integrand. The result of this procedure is

$$\varrho\dot{U}^l+\frac{1}{2}\varrho\sum_{m,n=0,1}^{\infty}\dot{k}^{l+m+n}\mathbf{v}_m\cdot\mathbf{v}_n+\left(U^l+\frac{1}{2}\sum_{m,n=0,1}^{\infty}k^{l+m+n}\mathbf{v}_m\cdot\mathbf{v}_n\right)\left(\dot{\varrho}+\varrho\varphi^\alpha_\alpha\right)$$
$$-\sum_{n=0,1}^{\infty}\left(\mathbf{m}^{l+n\,\alpha}|_\alpha-l\mathbf{m}^{l+n}+\varrho\bar{\mathbf{p}}^{l+n}\right)\cdot\mathbf{v}_n-\sum_{n=0,1}^{\infty}\mathbf{m}^{l+n\,\alpha}\cdot\mathbf{v}_{n,\alpha}=0\ , \tag{51}$$

in which we have added d'Alembert's acceleration terms to the corresponding original loads

$$\varrho\bar{\mathbf{p}}^l=\varrho\mathbf{p}^l-\varrho\sum_{m=0,1}^{\infty}k^{l+m}\dot{\mathbf{v}}_m\ . \tag{52}$$

The local set (51) of the generalized energy statement shall now be subjected to the invariance requirements already mentioned in Sect. 2, [49]. If we first superpose an arbitrary rigid body translation of constant velocity upon the original motion $\mathbf{v}^*$ (7) of the shell

$$\hat{\mathbf{v}}^*=\mathbf{v}^*+\overset{0}{\mathbf{v}}=\sum_{n=0,1}^{\infty}\theta^n\mathbf{v}_n+\overset{0}{\mathbf{v}}\quad\text{with}\quad\dot{\overset{0}{\mathbf{v}}}=\overset{0}{\mathbf{v}}_{,\alpha}=0\ , \tag{53}$$

we receive a scalar energy expression [32], from which we derive – because of the arbitrariness of $\overset{0}{\mathbf{v}}$ – the following conditions for the multi-director shell continuum:
the statement of conservation of mass

$$\left(\dot{\varrho} + \varrho\varphi^{\alpha}_{\alpha}\right) = 0 \quad \text{for} \quad l = 0, \quad \text{all} \quad \dot{k}^{l} = 0 \ , \tag{54}$$

the set of equations of motion

$$\mathbf{m}^{l\alpha}|_{\alpha} - l\mathbf{m}^{l} + \varrho\bar{\mathbf{p}}^{l} = \mathbf{0}, \quad l = 0, 1, ..\infty \ , \tag{55}$$

and the set of residual energy conservation

$$\varrho\dot{U}^{l} - \sum_{n=0,1}^{\infty}\left(n\mathbf{m}^{l+n}\cdot\mathbf{v}_{n} + \mathbf{m}^{l+n\,\alpha}\cdot\mathbf{v}_{n,\alpha}\right) = 0, \quad l = 0, 1, ..\infty \ . \tag{56}$$

Analogously, we superpose a steady rigid body rotation $\overset{0}{\boldsymbol{\omega}}$ upon the original motion $\mathbf{v}^{*}$

$$\hat{\mathbf{v}}^{*} = \mathbf{v}^{*} + \overset{0}{\boldsymbol{\omega}}\times\mathbf{r}^{*} = \sum_{n=0,1}^{\infty}\left(\theta^{n}\mathbf{v}_{n} + \overset{0}{\boldsymbol{\omega}}\times\theta^{n}\mathbf{d}_{n}\right) \quad \text{with} \quad \dot{\overset{0}{\boldsymbol{\omega}}} = \overset{0}{\boldsymbol{\omega}}_{,\alpha} = \mathbf{0} \ . \tag{57}$$

Requiring again energy conservation by application of the residual energy statements (56), we find

$$\sum_{n=0,1}^{\infty}\left(n\mathbf{m}^{l+n}\cdot\overset{0}{\boldsymbol{\omega}}\times\mathbf{d}_{n} + \mathbf{m}^{l+n\,\alpha}\cdot\overset{0}{\boldsymbol{\omega}}\times\mathbf{d}_{n,\alpha}\right) = 0 \ , \tag{58}$$

from which we construct due to the arbitrariness of $\overset{0}{\boldsymbol{\omega}}$ the following set of symmetry conditions:

$$\sum_{n=0,1}^{\infty}\left(n\mathbf{m}^{l+n}\times\mathbf{d}_{n} + \mathbf{m}^{l+n\,\alpha}\times\mathbf{d}_{n,\alpha}\right) = 0, \quad l = 0, 1, \ldots, \infty \ . \tag{59}$$

With this final transformation we have established all basic mechanical information from Sect. 3 consistent for a theory of multi-director shell continua. The external kinematics have been installed by (7), and the corresponding loads are given by (52). In the residual internal energies (56), we are able to identify pairs of dual internal mechanical variables contributing to the U^{l}. For the force variables, the equations of motion (55) in combination with the symmetry conditions (59) hold, while the kinematic equations are still hidden in $\mathbf{v}_{n}, \mathbf{v}_{n,\alpha}$ (56). All mechanical variables describe as state variables the deformed continuum at time t in a complete and consistent manner.

5
Decomposition with respect to the deformed reference surface

It is more convenient for our aims to work with vector components and component equations instead of vector variables and relations. Since we have considered solely the actual state of the shell structure at time t, we will now decompose all vector variables with respect to the basis (10) of the actual reference surface F.

We start the decomposition with the shell geometry, namely with the set of directors (5) on F

$$\mathbf{d}_{n} = d_{ni}\mathbf{a}^{i} = d^{i}_{n}\mathbf{a}_{i} \ , \tag{60}$$

from which – by virtue of the Weingarten formulae (17) – component forms of the director derivatives can be derived

$$\mathbf{d}_{n,\alpha} = \lambda_{ni\alpha}\mathbf{a}_{i} = \lambda_{n\,\beta\alpha}\mathbf{a}^{\beta} + \lambda_{n3\alpha}\mathbf{a}^{3} = \left(d_{n\,\beta}|_{\alpha} - d_{n3}b_{\alpha\beta}\right)\mathbf{a}^{\beta} + \left(d_{n3,\alpha} + d_{n\,\lambda}b^{\lambda}_{\alpha}\right)\mathbf{a}^{3} \ . \tag{61}$$

Under the use of (21, 22), the corresponding velocities can be established

$$\dot{\mathbf{d}}_n = \mathbf{v}_n = v_{ni}\mathbf{a}^i = \left(\dot{d}_{ni} - d_{nk}\varphi_i^k\right)\mathbf{a}^i = \left(\dot{d}_{ni} - d_{n\,\beta}\varphi_i^\beta\right)\mathbf{a}^i - d_{n3}\varphi_\beta^3\mathbf{a}^\beta \quad , \tag{62}$$

$$\dot{\mathbf{d}}_{n,\alpha} = \mathbf{v}_{n,\alpha} = \left(\dot{\lambda}_{ni\alpha} - \lambda_{nk\alpha}\varphi_i^k\right)\mathbf{a}^i = \left(\dot{\lambda}_{ni\alpha} - \lambda_{n\beta\alpha}\varphi_i^\beta\right)\mathbf{a}^i - \lambda_{n3\alpha}\varphi_\beta^3\mathbf{a}^\beta \quad . \tag{63}$$

If we specify the previous derivations to the position vector $\mathbf{r} = \mathbf{d}_0$, Eq. (6), of the reference surface F, we receive the expressions

$$\mathbf{d}_0 = \mathbf{r} = d_{0\beta}\mathbf{a}^\beta + d_{03}\mathbf{a}^3 \quad , \tag{64}$$

$$\mathbf{d}_{0,\alpha} = \mathbf{r}_{,\alpha} = \mathbf{a}_\alpha = \lambda_{0\beta\alpha}\mathbf{a}^\beta + \lambda_{03\alpha}\mathbf{a}^3 = a_{\alpha\beta}\mathbf{a}^\beta \quad , \tag{65}$$

and for their time derivatives some well-known connections from Sect. 2

$$\begin{aligned}\dot{\mathbf{d}}_0 &= \dot{\mathbf{r}} = \mathbf{v}_0 = v_{0\beta}\mathbf{a}^\beta + v_{03}\mathbf{a}^3,\\ \dot{\mathbf{d}}_{0,\alpha} &= \dot{\mathbf{r}}_{,\alpha} = \dot{\mathbf{a}}_\alpha = \varphi_{i\alpha}\mathbf{a}^i \quad .\end{aligned} \tag{66}$$

Let's proceed to the dynamic equilibrium. If we decompose the force variables $\mathbf{m}^{l\alpha}$, Eq. (47), $\mathbf{m}^l$, Eq. (48), and $\mathbf{p}^l$, Eq. (49), also with respect to the basis (10) of the surface F

$$\mathbf{m}^{l\alpha} = m_i^{l\alpha}\mathbf{a}^i = m^{l\alpha i}\mathbf{a}_i, \quad \mathbf{m}^l = m_i^l\mathbf{a}^i = m^{li}\mathbf{a}_i, \quad \bar{\mathbf{p}}^l = \bar{p}^{li}\mathbf{a}_i = \bar{p}_i^l\mathbf{a}^i \quad , \tag{67}$$

we are able to transform the equations of motion (55) under observation of (17) into the following component sets:

$$\begin{aligned}&m^{l\alpha\beta}|_\alpha - m^{l\alpha 3}b_\alpha^\beta - lm^{l\beta} + \varrho\bar{p}^{l\beta} = 0,\\ &m^{l\alpha 3}|_\alpha + m^{l\alpha\beta}b_{\alpha\beta} - lm^{l3} + \varrho\bar{p}^{l3} = 0, \quad l = 0, 1, \ldots, m \quad .\end{aligned} \tag{68}$$

Substitution of Eqs. (60, 61) and (67) into the symmetry conditions (59) furnishes under attention of Eq. (15) the provisional result

$$\begin{aligned}\sum_{n=0,1}^{\infty}\{&\mathbf{a}_3\varepsilon_{\beta\varepsilon}\left[nm^{l+n\,\beta}d_n^\varepsilon + m^{l+n\,\alpha\beta}\lambda_{n\,\alpha}^{\varepsilon}\right] + \mathbf{a}^\varrho\varepsilon_{\varrho\beta}\left[nm^{l+n\,\beta}d_n^3 - nm^{l+n\,3}d_n^\beta\right.\\ &\left.+m^{l+n\,\alpha\beta}\lambda_{n\,\alpha}^3 - m^{l+n\,\alpha 3}\lambda_{n\,\alpha}^\beta\right]\} = 0 \quad ,\end{aligned} \tag{69}$$

from which scalar multiplication with $\mathbf{a}^3$ delivers after some additional transformations from its first bracket $\bar{m}^{l(\alpha\beta)}$ as a new symmetric force variable

$$\bar{m}^{l(\alpha\beta)} = m^{l\alpha\beta} - \sum_{n=1,2}^{\infty}\left[nm^{l+n\,\beta}d_n^\alpha + m^{l+n\,\lambda\beta}\lambda_{n\,\lambda}^{\alpha}\right], \quad l = 0, 1, \ldots, m \quad . \tag{70}$$

A similar procedure with $\mathbf{a}^\lambda$ transforms its second bracket into the symmetry condition

$$\sum_{n=0,1}^{\infty}\left[nm^{l+n\,\alpha}d_n^3 - nm^{l+n\,3}d_n^\alpha + m^{l+n\,\lambda\alpha}\lambda_{n\,\lambda}^3 - m^{l+n\,\lambda 3}\lambda_{n\,\lambda}^{\alpha}\right] = 0, \quad l = 0, 1, \ldots, m \quad . \tag{71}$$

Finally, we decompose the scalar products of the energy conservation statement (56) using Eqs. (62, 63) as well as (67) again. If we consider after similar transformations in the provisional result

$$\varrho\dot{U}^l - \sum_{n=0,1}^{\infty}\left[nm^{l+n\,i}\dot{d}_{ni} + m^{l+n\,\alpha i}\dot{\lambda}_{ni\alpha} - \left(nm^{l+n\,i}d_{nk}\varphi_i^k + m^{l+n\,\alpha i}\lambda_{nk\alpha}\varphi_i^k\right)\right] = 0 \quad , \tag{72}$$

the symmetry conditions (70, 71), we receive the final set of the residual rate-of-energy equations

$$\varrho\dot{U}^l - \bar{m}^{l(\alpha\beta)}\dot{\alpha}_{(\alpha\beta)} - \sum_{n=1,2}^{\infty}\left[nm^{l+n\,i}\dot{d}_{ni} + m^{l+n\,\alpha i}\dot{\lambda}_{ni\alpha}\right] = 0, \quad l = 0, 1, ..\infty \ , \tag{73}$$

from which sets of constitutive relations (36) for the internal force variables can be deduced, in case of need.

From the energy conservation set (73), we observe the following ordering of dual internal dynamic and kinematic variables:

$$\bar{m}^{l(\alpha\beta)} : \dot{\alpha}_{(\alpha\beta)}; nm^{l+n\,i} : \dot{d}_{ni}; m^{l+n\,\alpha i} : \dot{\lambda}_{ni\alpha} \ .$$

The velocity kinematics (62, 63) appearing here are a consequence of the starting point (28) as rate-of-energy equation and are rather unfamiliar in solid mechanics. To relate them to usual displacement kinematics, we introduce

$$\alpha_{(\alpha\beta)} = \frac{1}{2}\left(a_{(\alpha\beta)} - \overset{0}{A}_{(\alpha\beta)}\right), \ \Delta d_{ni} = \left(d_{ni} - \overset{0}{D}_{ni}\right), \ \Delta\lambda_{ni\alpha} = \left(\lambda_{ni\alpha} - \overset{0}{\Lambda}_{ni\alpha}\right) \ , \tag{74}$$

as classical kinematic relations. In the respective brackets, the first variables describe basic geometrical quantities (60, 61) of the actual (deformed) configuration at time t, decomposed with respect to the actual basis (10) of F. The second variables are related to some initial (undeformed) configuration at time $t = 0$, also decomposed with respect to the base vectors $\{\overset{0}{\mathbf{a}}_\alpha, \overset{0}{\mathbf{a}}_3\}$ of the undeformed reference surface $\overset{0}{F}$. Formation of the time derivatives of (74)

$$\dot{\alpha}_{(\alpha\beta)} = \frac{1}{2}\dot{a}_{\alpha\beta}, \quad \dot{\overline{\Delta d_{ni}}} = \dot{d}_{ni}, \quad \dot{\overline{\Delta\lambda_{ni\alpha}}} = \dot{\lambda}_{ni\alpha} \ , \tag{75}$$

proves immediately the correct definition of the kinematic relations (74) in view of (73). If we now use the displacement vector $\mathbf{u}_0$ of the reference surface F, from (9) follows

$$\begin{aligned} \mathbf{u}_0 = \mathbf{d}_0 - \mathbf{D}_0 \quad \rightarrow \quad & \mathbf{d}_0 = \mathbf{D}_0 + \mathbf{u}_0 \\ & \mathbf{d}_{0,\alpha} = \mathbf{D}_{0,\alpha} + \mathbf{u}_{0,\alpha} \ , \end{aligned} \tag{76}$$

with

$$\begin{aligned} \mathbf{u}_0 &= u_0^\beta \overset{0}{\mathbf{a}}_\beta + u_0^3 \overset{0}{\mathbf{a}}_3, \\ \mathbf{u}_{0,\alpha} &= (u_0^\beta|_\alpha - u_0^3 \overset{0}{b}{}_\beta^\alpha)\overset{0}{\mathbf{a}}_\beta + (u_{0,\alpha}^3 + u_0^\lambda \overset{0}{b}_{\alpha\lambda})\overset{0}{\mathbf{a}}_3 \ . \end{aligned} \tag{77}$$

We are able thus to relate the position vector $\mathbf{d}_0$, its derivatives $\mathbf{d}_{0,\alpha}$ and the base vectors $\{\mathbf{a}_\alpha, \mathbf{a}_3\}$ of the deformed reference surface F to those ones of the undeformed surface $\overset{0}{F}$. Restricting ourselves for simplicity to the linear theory of small displacements, the final transformation reads

$$\mathbf{a}_i = \tilde{\varphi}_{.i}^k \overset{0}{\mathbf{a}}_k = \begin{bmatrix} \mathbf{a}_\alpha \\ \mathbf{a}_3 \end{bmatrix} = \begin{bmatrix} \delta_\alpha^\beta + u_0^\beta|_\alpha - u_0^3 \overset{0}{b}{}_\alpha^\beta & u_{0,\alpha}^3 + u_0^\lambda \overset{0}{b}_{\alpha\lambda} \\ -(u_{0,\cdot}^{3\beta} + u_0^\lambda \overset{0}{b}{}_\lambda^\beta) & 1 \end{bmatrix} \cdot \begin{bmatrix} \overset{0}{\mathbf{a}}_\alpha \\ \overset{0}{\mathbf{a}}_3 \end{bmatrix} \ , \tag{78}$$

which should not be confused with similar transformations (21, 22) of the base vector velocities. If we introduce the transformation tensors (78) into (74), we finally arrive at

$$\begin{aligned} \alpha_{(\alpha\beta)} &= \frac{1}{2}(u_{0\alpha}|_\beta + u_{0\beta}|_\alpha - 2u_{03}\overset{0}{b}_{\alpha\beta}), \\ \Delta d_{ni} &= \overset{0}{D}_{nk}(\tilde{\varphi}_{.i}^k - \delta_i^k) + u_{nk}\tilde{\varphi}_{.i}^k, \\ \Delta\lambda_{ni\alpha} &= \overset{0}{\Lambda}_{nk\alpha}(\tilde{\varphi}_{.i}^k - \delta_i^k) + u_{nk\alpha}\tilde{\varphi}_{.i}^k \ , \end{aligned} \tag{79}$$

with

$$u_{n\,\beta\alpha} = u_{n\,\beta}|_{\alpha} - u_{n3}\overset{0}{b}_{\alpha\beta}, \quad u_{n3\alpha} = u_{n3,\alpha} + u_{n\,\lambda}\overset{0}{b}{}^{\lambda}_{\alpha} \ . \tag{80}$$

Here, all displacement variables, the curvature tensor and the covariant derivatives are related – as usual for displacement kinematics in a Lagrangean setting – to the undeformed reference configuration $\overset{0}{F}$.

Finally, if we assume again the internal energy U in (73) to be solely a function of the internal kinematics $\alpha_{(\alpha\beta)}$, Δd_{ni}, $\Delta\lambda_{ni\alpha}$, Eq. (74), we are able to establish explicitly constitutive laws for the force variables (67, 70), as we did at the end of Sect. 3. For this step, we refer to [32].

With these transformations, we have gained the complete sets of fundamental equations for multi-director shell continua in component form, namely the mass conservation (54), the equations of motion (68) with two sets of symmetry conditions (70, 71), the kinematic relations (74, 79) with (60, 61) and the statements of energy conservation (73), all collected in Table 1. In all equations, except (74) and (76) to (80), only variables of the actual state at time t appear, the state variables of the problem. Compared to the classical treatment in 3D as sketched in Sec. 3, multi-director representations contain neither less nor more physical information. As mathematically complete integral transformation, the semi-discretization leads towards a consistent description of 3D solid mechanics problems, based on the actual reference surface F. Such description will allow the derivation of consistent asymptotic approximations, like classical, [32], or higher-order shell theories, [24]. Here, it will be used to deliver a more detailed mechanical insight into various shell simulation models than the 3D concept.

6
Two supplementary simplifications for shell models

As typical for the establishment of shell models, we have united in (47) the integral-transformed body forces $\mathbf{f}^*$ and tractions $\mathbf{t}^*$ on both shell faces into a set of external load variables for the multi-director shell continuum. Deleting mass and inertia effects, we retain from (47, 52)

$$\varrho\bar{\mathbf{p}}^l\sqrt{a} = \varrho\mathbf{p}^l\sqrt{a} = \left[\mathbf{t}^*\theta^l\sqrt{gg^{33}}\right]_{h^-}^{h^+}, \quad l = 0, 1, \ldots, \infty \ . \tag{81}$$

Intending to evaluate this term on both faces h^+, h^- of the shell continuum, we substitute the specialized stress expression (29)

$$\mathbf{t}^* = \sigma^{ij}n_i\mathbf{g}_j^* = \sigma^{3j}n_3\mathbf{g}_j^* \ , \tag{82}$$

and find

Table 1. Complete set of mechanical field statements for multi-director continua, equivalent to 3-D continuum mechanics

Multi-director representation of shell geometry:	$\mathbf{r}^* = \sum_n \theta^n\mathbf{d}_n(\theta^\alpha, t), \quad \mathbf{d}_n = d_{ni}\mathbf{a}^i \quad \mathbf{d}_{n,\alpha} = \lambda_{ni\alpha}\mathbf{a}^i$
Kinematics:	
External	$\mathbf{v}^* = \sum_n \theta^n\mathbf{v}_n(\theta^\alpha, t), \quad \mathbf{v}_n = v_{ni}\mathbf{a}^i = \dot{d}_{ni}\mathbf{a}^i$
	$\mathbf{u}^* = \sum_n \theta^n\mathbf{u}_n(\theta^\alpha, t), \quad \mathbf{u}_n = \mathbf{u}_{ni}\overset{\circ}{\mathbf{a}}{}^i$
Internal	$\alpha_{(\alpha\beta)}, \Delta d_{ni}, \Delta\lambda_{ni\alpha}$
Kinematic relations	$\alpha_{(\alpha\beta)} = \frac{1}{2}(\mathbf{a}_{\alpha\beta} - \overset{\circ}{\mathbf{A}}_{\alpha\beta}), \quad \Delta d_{ni} = d_{ni} - \overset{\circ}{\mathbf{D}}_{ni}, \quad \Delta\lambda_{ni\alpha} = \lambda_{ni\alpha} - \overset{\circ}{\mathbf{\Lambda}}_{ni\alpha}$
Force variables:	
External	$\rho\bar{\mathbf{p}}^l = \rho\mathbf{p}^l - \sum_m k^{l+m}\dot{\mathbf{v}}_m = \rho\bar{p}^{li}\mathbf{a}_i$
Internal	$\mathbf{m}^l = m^{li}\mathbf{a}_i, \quad \mathbf{m}^{l\alpha} = m^{l\alpha i}\mathbf{a}_i, \quad \bar{\mathbf{m}}^{l(\alpha\beta)}$
Equilibrium conditions	$m^{l\alpha\beta}|_\alpha - m^{l\alpha 3}b_\alpha^\beta - lm^{l\beta} + \rho\bar{p}^{l\beta} = 0, \quad m^{l\alpha 3}|_\alpha + m^{l\alpha\beta}b_{\alpha\beta} - lm^{l3} + \rho\bar{p}^{l3} = 0$
Symmetry statements	$\bar{m}^{l(\alpha\beta)} = m^{l\alpha\beta} - \sum_n (nm^{l+n\beta}d_n^\alpha + nm^{l+n\lambda\beta}\lambda_{n\cdot\lambda}^\alpha)$
	$\sum_n (nm^{l+n\alpha}d_n^3 - nm^{l+n3}d_n^\alpha + m^{l+n\lambda\alpha}\lambda_{n\cdot\lambda}^3 - m^{l+n\lambda 3}\lambda_{n\cdot\lambda}^\alpha) = 0$
Energy conservation:	$\rho\dot{U}^l - \bar{\mathbf{m}}^{l(\alpha\beta)}\dot{\alpha}_{(\alpha\beta)} - \sum_n (nm^{l+ni}\dot{d}_{ni} + m^{l+n\alpha i}\dot{\lambda}_{ni\alpha}) = 0$

$$\varrho \mathbf{p}^l = \left[\sqrt{\frac{gg^{33}}{a}} \sigma^{3j} n_3 \theta^l \mathbf{g}_j^* \right]_{h^-}^{h^+} . \tag{83}$$

If we further assume a typical thin shell space, [7], with

$$\mathbf{g}_j^* = \mu_j^k \mathbf{a}_k, \quad \mu_\beta^\lambda = \delta_\beta^\lambda - \theta b_\beta^\lambda, \quad \mu_j^3 = \mu_3^k = 0, \quad \mu_3^3 = 1 \ , \tag{84}$$

we derive the final load expression

$$\varrho \mathbf{p}^l = \left[\left(\sqrt{\frac{gg^{33}}{a}} \sigma^{3\beta} n_3 \mu_\beta^\lambda \theta^l \right) \mathbf{a}_\lambda + \left(\sqrt{\frac{gg^{33}}{a}} \sigma^{33} n_3 \theta^l \right) \mathbf{a}_3 \right]_{h^-}^{h^+} = \varrho p^{l\lambda} \mathbf{a}_\lambda + \varrho p^{l3} \mathbf{a}_3 \ . \tag{85}$$

In Fig. 4, we have illustrated this expression for the case of a flat plate, described by an orthonormal base $|\mathbf{a}_i| = 1$, $\sqrt{gg^{33}/a} = 1$, and portrayed in a $\theta^2 = \text{const.}$ cross section. The zeroth load moments ϱp^{01}, ϱp^{03} (load resultants) are distributed half on each face and the first load moments are plotted right beside. We observe that by adding or subtracting both loading terms, each desired load concentration on both faces can be described: the acting forces (on the upper) as well as bearing forces (on the lower face). For shell structures, the zeroth and the first load moments are essential external force variables. Generally, because of lack of physical significance, all higher load moments are to be deleted

$$\varrho \mathbf{p}^l = 0 \quad \text{for} \quad l \geq 2 \ . \tag{86}$$

Next, we cast a more detailed look into the equations of motion (68) and discover two different sets of internal force variables: first, (48) as moments $\mathbf{m}^{l\alpha}$, the stresses of which act in θ^α-directions

$$\mathbf{m}^{l\alpha} \sqrt{a} = \int_{h^-}^{h^+} \mathbf{T}^{*\alpha} \theta^l \, \mathrm{d}\theta \ , \tag{87}$$

and second, the moments $\mathbf{m}^l$ (49), the stresses of which act in the θ^3-direction

$$\mathbf{m}^l \sqrt{a} = \int_{h^-}^{h^+} \mathbf{T}^{*3} \theta^{l-1} \, \mathrm{d}\theta \ . \tag{88}$$

Let us emphasize that the classical way of establishing equilibrium conditions by equilibrating virtually cut out shell elements never can exhibit the latter variables (88). Have they been overseen in the majority of shell researches up to now?

For an answer, we introduce (29)

$$\mathbf{T}^{*i} = \sqrt{g} \sigma^{ij} \mathbf{g}_j^* \ , \tag{89}$$

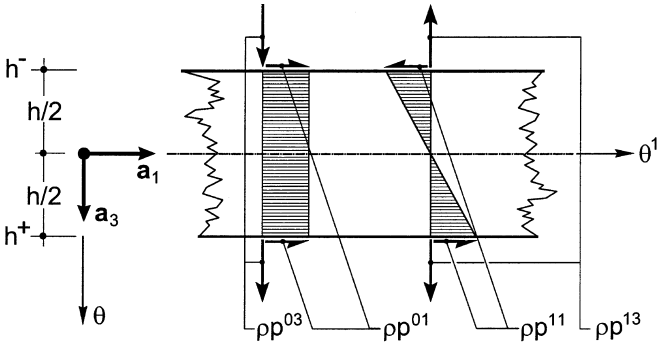

Fig. 4. Cross section of a plate with load resultant and first order load moment

into both sets of moments (87, 88). If we again specify both terms onto the typical shell space (84), we discover by comparison of the second term of (90) with the first term of (91)

$$\mathbf{m}^{l\alpha} = \int_{h^-}^{h^+} \sqrt{\frac{g}{a}} \sigma^{\alpha\beta} \theta^l \mu_\beta^\lambda \, \mathrm{d}\theta \mathbf{a}_\lambda + \int_{h^-}^{h^+} \sqrt{\frac{g}{a}} \sigma^{\alpha 3} \theta^l \, \mathrm{d}\theta \mathbf{a}_3 = m^{l\alpha\lambda} \mathbf{a}_\lambda + m^{l\alpha 3} \mathbf{a}_3 \ , \tag{90}$$

$$\mathbf{m}^{l} = \int_{h^-}^{h^+} \sqrt{\frac{g}{a}} \sigma^{3\beta} \theta^{l-1} \mu_\beta^\lambda \, \mathrm{d}\theta \mathbf{a}_\lambda + \int_{h^-}^{h^+} \sqrt{\frac{g}{a}} \sigma^{33} \theta^{l-1} \, \mathrm{d}\theta \mathbf{a}_3 = m^{l\lambda} \mathbf{a}_\lambda + m^{l3} \mathbf{a}_3 \ , \tag{91}$$

for very thin shells ($\mu_\beta^\lambda = \delta_\beta^\lambda$), and because of interchangeability of the stress tensor indices ($\sigma^{\alpha 3} = \sigma^{3\alpha}$), the approximative result

$$m^{l\,\lambda 3} \approx m^{l+1\,\lambda} \ . \tag{92}$$

This statement, exactly valid only in the limit $h \to 0$, can be derived more rigorously including its bounds following from the symmetry condition (71). To answer the above posed question: the $\mathbf{a}_3$-components of (87) can be transformed into the $\mathbf{a}_\lambda$-components of (88), and the latter are generally included in the first ones, as the corresponding kinematics.

7
Classical shell theories and error bounds

The equations for multi-director continua, summarized at the end of Sect. 5, form hierarchical sets ($l, m, n = 0, 1, \to \infty$) of variables and conditions. As mathematically rigorous integral transformations, they solve for $l, m, n \to \infty$ any problem of 3D continuum mechanics with identical solution quality. Starting from $l, m, n = 0$, all subsets of same hierarchical level (l, m, n) converge so that their solutions approach the 3D counterparts in an asymptotic manner for $h \to 0$, [29]. This recognition is the key idea of the transition from multi-director continuum theories to classical shell models.

Classical shell theories approximate the mechanical behavior of surface-like solids by the deformational properties of surfaces, namely by stretching and bending. To express it more precisely: thin shells are defined as approximations of continua, the kinematics of which are identical with those of a Cosserat surface. Cosserat surfaces characterize surfaces with stiffness (and mass) properties, such that their states of deformation can be determined uniquely by tools of differential geometry of surfaces, [35].

The zeroth and first moments of our multi-director representation in Table 1, as resultants and linear moments of variables and conditions, will follow the given definition to a large extent. Small perturbations appear from all transverse effects, like transverse shear and normal forces, and their corresponding strain measures. By estimates using spectral tensor norms, [28, 32], the influence of these perturbations is attempted to be kept small in shell theories.

Because of the given definition, classical shell theories use the simple representation (4) from differential geometry, here for the undeformed shell

$$\mathbf{R}^* = \mathbf{D}_0 + \theta \mathbf{D}_1, \quad \mathbf{D}_n = \mathbf{0} \quad \text{for} \quad n \geq 2 \ , \tag{93}$$

with

$$\mathbf{D}_0 \text{ arbitrary}, \quad \mathbf{D}_1 = \overset{0}{\mathbf{a}}_3, \quad \overset{0}{\Lambda}_{1\beta\alpha} = -\overset{0}{b}_{\alpha\beta}, \quad \overset{0}{\Lambda}_{13\alpha} = 0 \ . \tag{94}$$

Due to the suppression of the thickness stretch Δd_{13}, the displacement representation (9) reads

$$\mathbf{u}^* = \mathbf{u}_0 + \theta \mathbf{u}_1 = u_{oi} \overset{0}{\mathbf{a}}{}^i + \theta u_{1\alpha} \overset{0}{\mathbf{a}}{}^\alpha \ . \tag{95}$$

Introducing this into (79), we find expressions for the first strain tensor, the transverse shear measure and the second strain tensor of F

$$\alpha_{(\alpha\beta)} = \frac{1}{2}\left(u_{0\alpha|\beta} + u_{0\beta|\alpha} - 2u_{03}\overset{0}{b}_{\alpha\beta}\right),$$

$$\Delta d_{1\alpha} = \gamma_\alpha = u_{1\alpha} + u_{03,\alpha} + u_{0\lambda}\overset{0}{b}_{\lambda\alpha}, \tag{96}$$

$$\Delta\lambda_{1\beta\alpha} = \beta_{\beta\alpha} = u_{1\beta|\alpha} - u_{0\lambda|\beta}\overset{0}{b}{}^{\lambda}_{\alpha} + u_{03}\overset{0}{b}{}^{\lambda}_{\alpha}\overset{0}{b}_{\lambda\beta} \ ,$$

if – for a linear theory – all quadratic displacement terms are neglected. We additionally receive as internal kinematics $\Delta\lambda_{13\alpha}$, the strain measure of the transverse shear moments, due to stresses $\sigma^{\alpha 3}$ linearly distributed over the thickness. It has been proven, [28, 30], that $\Delta\lambda_{13\alpha}$ has a negligible order of magnitude compared to (96) in the validity range of shell theories. With (96), we observe from the energy conservation statement (73) the existence of the following force variables:

$m^{l\alpha\beta}$:	$m^{0\alpha\beta}$	the tensor of in-plane stress resultants,
	$m^{1\alpha\beta}$	the tensor of in-plane stress moments,
$m^{l\alpha 3}$:	$m^{0\alpha 3} = m^{1\alpha}$	the vector of transverse shear forces, comp. (92).

For an orthogonal basis, Fig. 5 illustrates these force variables together with their stress distributions, applying their definitions (48, 49).

In a similar systematic manner, all basic variables and equations of classical shell theory can be re-derived from the multi-director basis in Table 1, applying the mentioned tensor norm estimates. Without repeating these derivations, [32], the results are summarized in Table 2, both in multi-director and classical notation.

Classical shell theory is an asymptotic approximation of 3D continuum mechanics for $h \to 0$, which is expressed by the error measure

$$\theta = \max\left\{\frac{h}{L}, \frac{h}{L_W}, \sqrt{\frac{h}{R}}, \sqrt{\eta}\right\} \quad , \quad |\gamma_{ij}| \approx |\dot{\gamma}_{ij}| \leq \eta \ll 1 \ . \tag{97}$$

Herein, h denotes the shell thickness; L its smallest length dimension; R the smallest radius of curvature of F; L_W the smallest wave-length of deformation pattern, [28]; η represents the norm of the maximum strain. Classical shell theory will deliver reliable results only if this error measure θ remains small. As restricted 'resultant-and-first-order-moment-map' of the 3D model, this can be expected with sufficient accuracy only for suitable distance from all perturbations, like concentrated loads, shell bearings, macro-damages or abrupt thickness changes. Obviously, constitutive laws for plane stress are required.

From the summary in Table 2, all well-known versions of the classical shell theory can be derived, supplementing explicit constitutive laws, its variational formulations and usual simplifications. The interested reader is referred to [7].

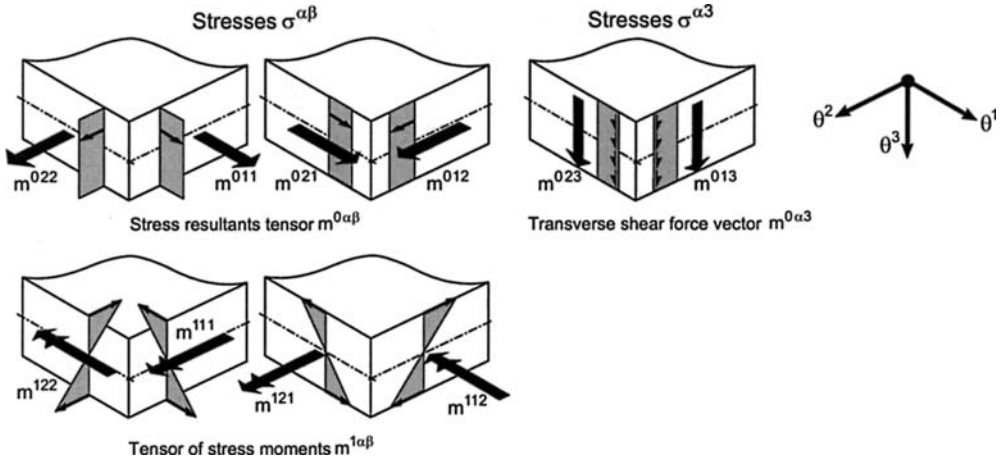

Fig. 5. Internal force variables of classical five-parameter (Reissner-Mindlin) shell theory

Table 2. Classical linear shear deformable shell theory (Reissner-Mindlin), multi-director notation (right) and usual tensor notation (left)

Representation of shell geometry:		
	$\mathbf{R}^* = \mathbf{D}_0 + \theta \overset{\circ}{\mathbf{a}}_3$	$= \mathbf{D}_0 + \theta \mathbf{D}_1 = \mathrm{D}_{0.}^{i} \overset{\circ}{\mathbf{a}}^i + \theta \mathrm{D}_{1.}^{3} \overset{\circ}{\mathbf{a}}_3$
Kinematics:		
External	$\mathbf{u}^* = \mathbf{u} + \theta \mathbf{w}$	$= \mathbf{u}_0 + \theta \mathbf{u}_1 = u_{0i} \overset{\circ}{\mathbf{a}}^i + \theta u_{1\alpha} \mathbf{a}^\alpha$
Internal	$\{\alpha_{(\alpha\beta)}, \gamma_\alpha, \beta_{(\alpha\beta)}\}$	$\{\alpha_{(\alpha\beta)}, \Delta d_{1\alpha}, \Delta\lambda_{1(\alpha\beta)}\}$
Kinematic relations	$\alpha_{(\alpha\beta)} = \frac{1}{2}(u_{\alpha l\beta} + u_{\beta l\alpha} - 2u_3 \overset{\circ}{b}_{\alpha\beta})$	
	$\gamma_\alpha = w_\alpha + u_{3,\alpha} + u_\lambda \overset{\circ}{b}{}^{\lambda}_{\alpha}$	
	$\beta_{(\alpha\beta)} = \frac{1}{2}(w_{\alpha l\beta} + w_{\beta l\alpha} - u_{\lambda l\alpha} \overset{\circ}{b}{}^{\lambda}_{\beta} - u_{\lambda l\beta} \overset{\circ}{b}{}^{\lambda}_{\alpha} + 2u_3 \overset{\circ}{b}{}^{\lambda}_{\alpha} \overset{\circ}{b}_{\lambda\beta})$	
Force variables:		
External	$\mathbf{p}, \mathbf{c}$	$\rho \mathbf{p}^0 = \rho p^{0i} \overset{\circ}{\mathbf{a}}_i, \quad \rho \mathbf{p}^1 = \rho p^{1\alpha} \mathbf{a}_\alpha$
Internal	$\{n^{\alpha\beta}, q^\alpha, m^{(\alpha\beta)}\}$	$\{m^{0\alpha\beta}, m^{1\alpha}, m^{1(\alpha\beta)}\}$
Equilibrium conditions	$n^{\alpha\beta}\vert_\alpha + q^\alpha \overset{\circ}{b}{}^{\beta}_{\alpha} + p^\beta = 0$	
	$q^\alpha\vert_\alpha + n^{\alpha\beta} \overset{\circ}{b}_{\alpha\beta} + p^3 = 0$	
	$m^{(\alpha\beta)}\vert_\alpha - q^\beta + c^\beta = 0$	
Symmetry conditions	$\bar{n}^{(\alpha\beta)} = n^{\alpha\beta} + m^{(\alpha\lambda)} \overset{\circ}{b}{}^{\beta}_{\lambda}$	
Energy conservation:	$\rho \dot{U}^l = \bar{n}^{(\alpha\beta)} \dot{\alpha}_{\alpha\beta} + m^{(\alpha\beta)} \dot{\beta}_{(\alpha\beta)} + q^\alpha \dot{\gamma}_\alpha$	

8
Solid shell elements and locking defects

The key aim of the classical shell theory was the surface-like approximation of kinematics; the price to pay were plane-stress material restrictions and inherent modeling errors (97). Consequently, the development of 'degenerated 3D' or 'solid shell' concepts intended to overcome these deficiencies by a linear displacement interpolation over the thickness, applied directly in the 3D kinematic relations. The aim of this concept are low-order continuum elements, yet capable of full 3D constitutive laws.

There has been much research in the field of hierarchical shell formulations conducted during the recent decades, [1, 4, 15]. The theories include higher-order models in thickness direction and eliminate locking defects by use of the so-called *p*-version. Especially with respect to adaptive mesh refinement strategies, [22], we restrict our investigation in this contribution to the classical low-order approximation concept.

In our systematics, such a concept turns out to be a complete zeroth- and first-order approximation of the multi-director theory as given in Table 1, opposite to the incomplete first-order approximation of classical shell theory. The semi-discretization in the thickness direction θ^3 applied in Sect. 3 is interrupted now after $l = 1$, which corresponds to the linear displacement interpolation. The deformed shell geometry (4) is approximated by

$$\mathbf{r}^* = \mathbf{d}_0 + \theta \mathbf{d}_1 \quad , \tag{98}$$

and the velocity (7) as well as the displacement vector (9), both external kinematics, are given by

$$\mathbf{v}^* = \mathbf{v}_0 + \theta \mathbf{v}_1, \quad \mathbf{u}^* = \mathbf{u}_0 + \theta \mathbf{u}_1 \quad . \tag{99}$$

In contrast to the classical shell theory, vectors $\mathbf{d}_1, \mathbf{v}_1$ and $\mathbf{u}_1$ now contain components also in $\mathbf{a}^3$-direction; in case of $\mathbf{u}_1$ generally denoted as thickness stretch

$$\mathbf{u}^* = u_{oi} \overset{0}{\mathbf{a}}{}^i + \theta u_{1i} \overset{0}{\mathbf{a}}{}^i = u_{oi} \overset{0}{\mathbf{a}}{}^i + \theta u_{1\alpha} \overset{0}{\mathbf{a}}{}^\alpha + \theta u_{13} \overset{0}{\mathbf{a}}{}^3 \quad . \tag{100}$$

The resulting solid shell elements according to Fig. 1 are controlled from nodal points with displacement DOFs along their coupling boundaries. To line out the parallels, we project the displacement vector $\mathbf{u}^*$, Eq. (100), from the middle surface F to the intersection points of the director $\mathbf{d}_1$ with both faces of the shell, s. Fig. 6,

$$\theta = \pm \frac{h}{2}: \quad \mathbf{u}^* = \mathbf{u}_0 \pm \frac{h}{2} \mathbf{u}_1 = u_{oi} \overset{0}{\mathbf{a}}{}^i \pm \frac{h}{2} u_{1i} \overset{0}{\mathbf{a}}{}^i = (u_{oi} \pm \frac{h}{2} u_{1i}) \overset{0}{\mathbf{a}}{}^i \quad , \tag{101}$$

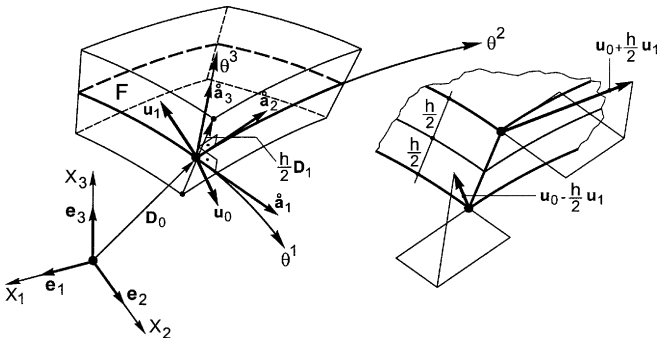

Fig. 6. Projection of displacement vector $\mathbf{u}^*$ from middle surface to both shell faces

and choose both displacements as new (solid shell) DOFs

$$\mathbf{u}^*\left(\theta=\frac{h}{2}\right)=\left(u_{oi}+\frac{h}{2}u_{1i}\right)\overset{0}{\mathbf{a}}{}^i, \quad \mathbf{u}^*\left(\theta=-\frac{h}{2}\right)=\left(u_{oi}-\frac{h}{2}u_{1i}\right)\overset{0}{\mathbf{a}}{}^i \ . \tag{102}$$

Such an exchange of external kinematic variables does not alter the mechanical content of the concept. For special purposes, like contact problems, [44], or analysis of interface effects, [50], also classical shell theories have been developed using quantities in (102) as DOFs. For solid shell concepts, [10, 21, 26, 39], these kinematics are the natural choice: they apply linear displacement interpolation over the thickness directly in the 3D kinematic relations, and thus receive an immediate interpolation map with the face displacements as parameters. This clearly is the shortest access to numerical analysis codes. Our way, however, interpreting solid shells as consistent complete first-order approximations of multi-director theories, delivers deeper insight into structure and kinematic capability of solid shells.

For small displacements, we follow the derivation of Sec. 7, for a complete first-order approximation. With the undeformed shell geometry (93, 94) and the displacement vector (100) as external kinematics, we receive from (79) the following conditions for the internal kinematics, [32]:

$$\begin{aligned}
&\alpha_{(\alpha\beta)}=\frac{1}{2}\left(u_{0\alpha|\beta}+u_{0\beta|\alpha}-2u_{03}\overset{0}{b}{}_{\alpha\beta}\right) \ , \\
&\Delta d_{1\alpha}=u_{1\alpha}+u_{03,\alpha}+u_{0\lambda}\overset{0}{b}{}^{\lambda}_{\alpha} \ , \\
&\Delta d_{13}=u_{13} \ , \\
&\Delta\lambda_{1\beta\alpha}=u_{1\beta|\alpha}-u_{13}\overset{0}{b}{}_{\alpha\beta}-u_{0\lambda|\beta}\overset{0}{b}{}^{\lambda}_{\alpha}+u_{03}\overset{0}{b}{}^{\lambda}_{\alpha}\overset{0}{b}{}_{\lambda\beta} \ , \\
&\Delta\lambda_{13\alpha}=u_{13,\alpha}+\Delta d_{1\lambda}\overset{0}{b}{}^{\lambda}_{\alpha} \ .
\end{aligned} \tag{103}$$

From these terms, the first strain tensor $\alpha_{(\alpha\beta)}$ of F, its shear deformation measure $\Delta d_{1\alpha}$ for constant shear stress $\sigma^{\alpha 3}$ and the nonsymmetrized part $\Delta\lambda_{1\beta\alpha}$ of the second strain tensor, enriched by u_{13}, are known from classical shell theory. They are completed by the thickness stretch Δd_{13} and by the strain measure $\Delta\lambda_{13\alpha}$ for shear stress profiles $\sigma^{\alpha 3}$ linear over the thickness, while the earlier 'degenerated' shell concept, [2, 41], suppressed in (103) Δd_{13} and $\Delta\lambda_{13\alpha}$. In case of a linear theory, there are no couplings to further higher-order kinematics. If we then order from (73) the corresponding force variables for solid shell theories, we get Fig. 7.

As Fig. 7 elucidates, in comparison to Fig. 5, the concept of solid shells enlarges the deformability of classical shell theory by two new deformation modes, namely the thickness stretch Δd_{13} and the shear strain measure $\Delta\lambda_{13\alpha}$. This cannot be judged as a very striking improvement apart from Δd_{13}, since generally $\Delta\lambda_{13\alpha}$ will not be required often.

Consequently, low-order solid shell elements, [25, 26, 33], may exhibit similarly severe (and more) defects as classical shell elements, known today as stiffness locking phenomena. The most widespread isoparametric hexahedron-element with eight nodes and tri-linear interpolation is sensitive to shear and curvature locking. Shear locking is due to the fact that pure bending of the element is infected by incorrect shear modes. The well-approved remedy, proposed in [16], cures this defect by evaluating correct (equilibrium) transverse shear strains

at collocation points and interpolating them throughout the element in more suitable continuity, Fig. 8. Curvature locking in curved geometry provides parasitic normal strains ε_{33}. To overcome this locking defect, a further assumed strain concept, [9], evaluates the correctly determined normal strains in the nodal points and interpolates them by bi-linear interpolation throughout the element.

Further, the membrane behavior of such element can be severely disturbed by volumetric locking, [13, 9, 10], a combination of Poisson and membrane locking. To cure them, the first mentioned paper proposes the enhancement of the compatible strain fields by over the thickness linearly varying normal strains ε_{33}, and by additional membrane strains $\{\varepsilon_{11}, \varepsilon_{12} = \varepsilon_{21}, \varepsilon_{22}\}$. According to Fig. 7, the first enhancement does not belong to a consistent first-order approximation, $l = 0, 1$. The second one simply improves the in-plane deformability of the element by anti-symmetric modes in the isoparametric element map.

Such enhanced strain fields are caused by the fact that the deformability of the solid shell concept as a complete first-order approximation of the multi-director theory is still insufficient. All enhanced strains are incompatible with the strains derived from the displacement fields. In order to avoid their participation to the internal energy, and thus a violation of energy conservation, they have to be assumed orthogonal to the free assumed

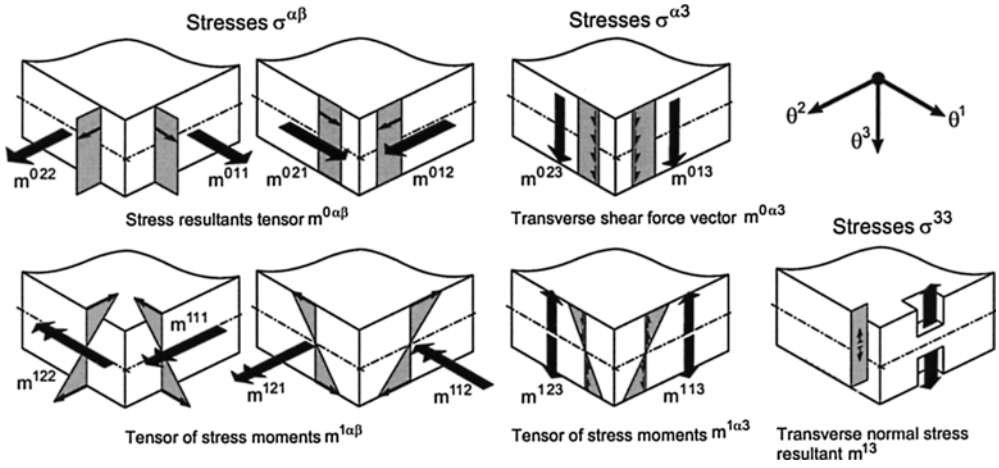

Fig. 7. Total set of internal force variables of the complete first order approximation (six-parameters theory)

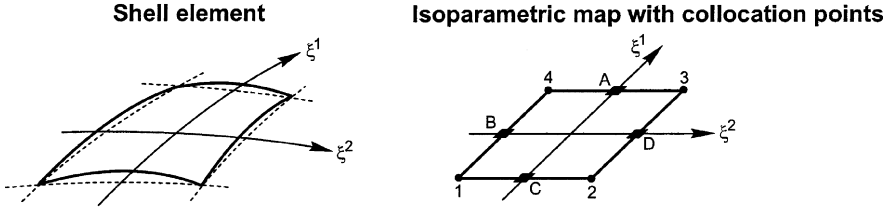

ANS - concept:

Shear locking:

$$\begin{bmatrix} 2\varepsilon_{13} \\ 2\varepsilon_{23} \end{bmatrix} = \begin{bmatrix} (1+\xi^1)\,\varepsilon_{13,A} + (1-\xi^1)\,\varepsilon_{13,C} \\ (1-\xi^2)\,\varepsilon_{23,B} + (1+\xi^2)\,\varepsilon_{23,D} \end{bmatrix}$$

Curvature locking:

$$\left[4\varepsilon_{33}\right] = \begin{bmatrix} (1-\xi^1)(1-\xi^2) \\ (1-\xi^1)(1+\xi^2) \\ (1+\xi^1)(1+\xi^2) \\ (1+\xi^1)(1-\xi^2) \end{bmatrix}^{\mathrm{T}} \cdot \begin{bmatrix} \varepsilon_{33,1} \\ \varepsilon_{33,2} \\ \varepsilon_{33,3} \\ \varepsilon_{33,4} \end{bmatrix}$$

EAS - concept: $\boldsymbol{\varepsilon} = \boldsymbol{\varepsilon}^c(\mathbf{u}) + \boldsymbol{\varepsilon}(\boldsymbol{\alpha})$

Transversal strain enhancement:

$$\left[\tilde{\varepsilon}_{33}\right] = \frac{\theta^3}{\sqrt{G}} \begin{bmatrix} 1 & \xi^1 & \xi^2 & \xi^1\xi^2 \end{bmatrix} \cdot \begin{bmatrix} \alpha_{T1} \\ \vdots \\ \alpha_{T4} \end{bmatrix}$$

Membrane strain enhancement:

$$\begin{bmatrix} \tilde{\varepsilon}_{11} \\ \tilde{\varepsilon}_{22} \\ \tilde{\varepsilon}_{12} \end{bmatrix} = \frac{\mathbf{T}}{\sqrt{G}} \begin{bmatrix} \xi^1 & 0 & 0 & 0 & \xi^1\xi^2 & 0 & 0 \\ 0 & \xi^2 & 0 & 0 & 0 & \xi^1\xi^2 & 0 \\ 0 & 0 & \xi^1 & \xi^2 & 0 & 0 & \xi^1\xi^2 \end{bmatrix} \cdot \begin{bmatrix} \alpha_{M1} \\ \vdots \\ \alpha_{M7} \end{bmatrix}$$

Fig. 8. Assumed-natural-strain concept (ANS) and enhanced-assumed-strain concept (EAS)

stress fields. Additional free parameters of the enhanced strain fields are condensed out on the element level.

Although heavily attacked at their beginning from view points of calculus of variation, solid shell elements with ANS- and/or EAS-supplements, as summarized in Fig. 8, are accepted today and considered as very robust, [10, 26]. Because of their uncomplicated theoretical background, easy coding, general applicability for linear and nonlinear responses, and simple kinematics, they probably will dominate future shell analyses to a large extent.

9
Higher-order shell theories – an erroneous deadlock?

Locking effects and modeling deficiencies may have their origin in the lack of suitable deformability in certain theories and elements. A rather classical remedy is the application of higher-order shell theories, [24, 42]. For a consistent second-order approximation ($l = 0, 1, 2$), the deformed geometry (4) is described e.g. by

$$\mathbf{r}^* = \mathbf{r}_0 + \theta \mathbf{r}_1 + \theta^2 \mathbf{r}_2 \ , \tag{104}$$

and the displacement vector (9) consequently by

$$\mathbf{u}^* = \mathbf{u}_0 + \theta \mathbf{u}_1 + \theta^2 \mathbf{u}_2 \ . \tag{105}$$

If we would now re-evaluate all strain variables (79) of this approximation and then, by comparison with (73), identify the corresponding internal force variables, we would receive the variety pictured in Fig. 9. In addition to those force variables of the solid shell concept shown in Fig. 7, we discover now the tensor of bi-moments $m^{2\alpha\beta}$ for quadratic in-plane stresses $\sigma^{\alpha\beta}$, the vector of transverse bi-moments $m^{2\alpha 3}$ for quadratic stress profiles $\sigma^{\alpha 3}$, and the transverse normal stress moment m^{23} for stress contributions σ^{33} linear over the thickness. One easily observes that some of the anti-locking deformability, Δd_{23}, has been added, but probably not all.

For a first insight into a complete second-order shell approximation, we consistently write the equations of motion (68) for $l = 0, 1, 2$

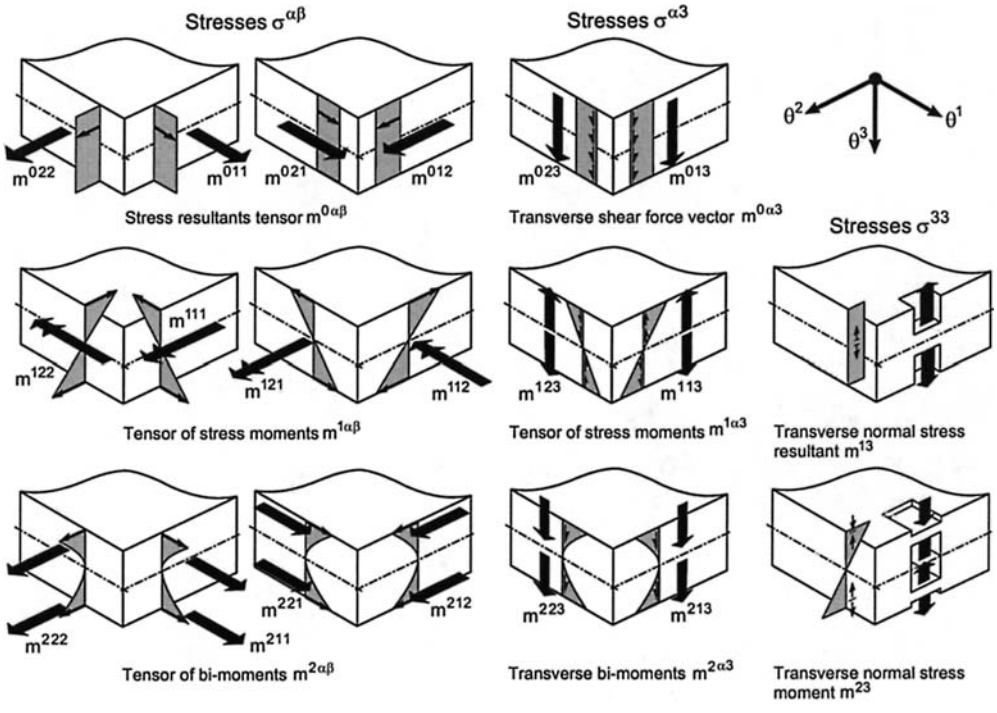

Fig. 9. Total set of internal force variables of complete second-order approximation (nine-parameters theory)

$$
\begin{array}{lllllllllll}
l=0: & m^{0\alpha\beta}|_{\alpha} & - & m^{0\alpha 3}b^{\beta}_{\alpha} & & & + & \varrho\bar{p}^{0\beta} & = & 0\ , \\
 & m^{0\alpha 3}|_{\alpha} & + & m^{0\alpha\beta}b_{\alpha\beta} & & & + & \varrho\bar{p}^{03} & = & 0\ , \\
l=1: & m^{1\alpha\beta}|_{\alpha} & - & m^{1\alpha 3}b^{\beta}_{\alpha} & - & m^{1\beta} & + & \varrho\bar{p}^{1\beta} & = & 0\ , \\
 & m^{1\alpha 3}|_{\alpha} & + & m^{1\alpha\beta}b_{\alpha\beta} & - & m^{13} & + & \varrho\bar{p}^{13} & = & 0\ , \\
l=2: & m^{2\alpha\beta}|_{\alpha} & - & m^{2\alpha 3}b^{\beta}_{\alpha} & - & 2m^{2\beta} & + & \varrho\bar{p}^{2\beta} & = & 0\ , \\
 & m^{2\alpha 3}|_{\alpha} & + & m^{2\alpha\beta}b_{\alpha\beta} & - & 2m^{23} & + & \varrho\bar{p}^{23} & = & 0\ .
\end{array}
\tag{106}
$$

If by use of (92) we exchange all force components $m^{l+1\lambda}$ with $m^{l\lambda 3}$, delete all higher-order load moments $\varrho\bar{p}^{li}$ for $l \geq 2$ in consequence of (86), expand the scheme to a third-order theory and rearrange some terms, we arrive at the result of Table 3.

The first three lines in Table 3 express the classical shell theory and the first four lines the solid shell concept. These latter four lines model the load response in terms of integral transformed primary, e. g. load-dependent stress variables. All further lines add self-equilibrating states of stress, secondary stresses, similar to classical edge perturbations, again in terms of integral transforms to the initial primary ones. In classical shell theory, membrane and bending effects are coupled by the transverse shear force vector $m^{0\alpha 3}$ as resultants of $\sigma^{\alpha 3}$. Obviously in case of higher-order approximations, all coupling terms to the respective next hierarchical step in Table 3 are formed by vector quantities $m^{l\alpha 3}$, $l \geq 1$, moments of suitable order of $\sigma^{\alpha 3}$.

Can there be weighted up against each other the pros and cons of second-order shell theories, although only few numerical experiences with higher-order approximations are available? A second-order theory will improve the Poisson locking of solid shell concepts, for the price of additional nodes over the shell thickness or higher-order kinematics. A clear disadvantage is the heuristic derivation of such theories, [5, 40], which lack systematic convergence analysis as well as error bounds, [11]. And, finally, no systematic research is known regarding decisions, whether a third -or even higher -order approximation is required when a second-order one turns out to be insufficient.

All these problems find an interesting alternative by application of multi-layered packages of shell elements.

10
Real multi-layered shell concepts and 3D convergence

In the analysis of sandwich shells, Gauss-point integration has to be extended over sublayers of different material properties. Artificial sublayers are generally applied also for layer-wise integration in the analysis of inelastic shell response. It is an obvious idea to expand such concepts of natural or artificial layering towards an external refinement, in which additional DOFs at the coupling points, see Fig. 1, are introduced, to increase the deformability of the layered package. By engineering intuition, or by surveying the force variables of the complete second-order approximation in Fig. 9, or by a critical review of the ANS- and EAS-concepts shown in Fig. 8, we anticipate that such refinements, when used in sufficient number, will cure locking.

As illustrated in Fig. 10, such real multi-layer theories are formed by packages of single-layer shell elements coupled at their nodes. If the global reference surface F_G in Fig. 10 is identified

Table 3. Hierarchial set of equations of motion for multi-director theory up to $l = 3$

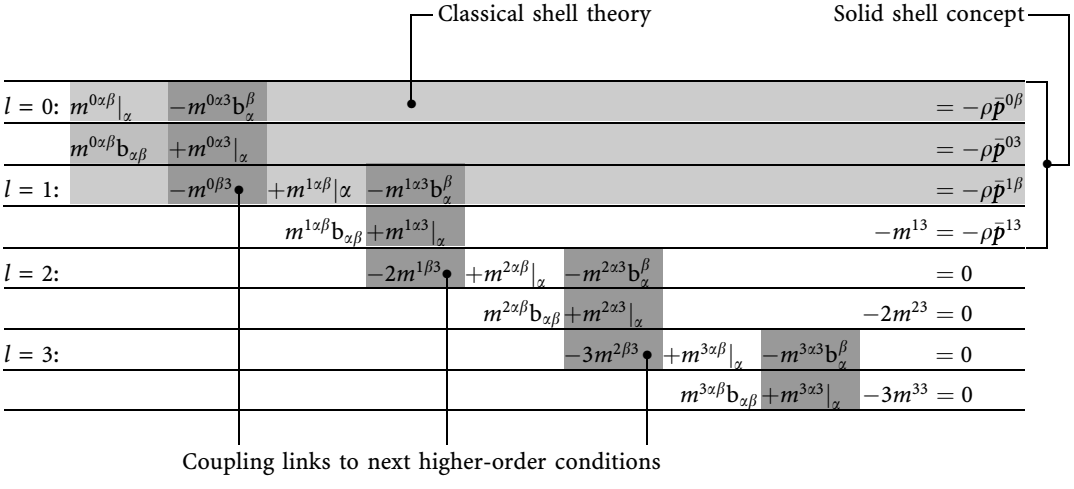

with the local one of the layer $L = 1$, chosen on its lower face, the position vector $\mathbf{r}^*$ of an arbitrary point P^* can be described by

$$\mathbf{r}^* = \sum_{L=0}^{N} \sum_{n=0,1}^{\infty} \theta_L^n \mathbf{d}_{Ln}(\theta^\alpha, t) = \mathbf{r} + \sum_{L=1}^{N} \sum_{n=1,2}^{\infty} \theta_L^n \mathbf{d}_{Ln}(\theta^\alpha, t) \ , \tag{107}$$

with point P^* in layer $J < N$ for

$$\begin{aligned} &L = 1, 2, \ldots, J-1: \quad \theta_L = h_L \ , \\ &L = J: \qquad\qquad\quad \text{actual } \theta_L \ . \end{aligned}$$

Each single layer may be modeled by a multi-director shell theory of arbitrary order $l \geq 1$.

To derive a concept of practical applicability, we introduce the following limit: the single layer in Fig. 10 shall be modeled by a simple solid shell element, e. g. by an eight-noded hexahedron with linear displacement interpolation over the thickness. ANS- or EAS-supplements are recommended. Each single layer may be of arbitrary thickness, leaving its number open. Equal thickness usually is assumed for adaptivity, with suitable error estimates and transition elements, [22], a topic, which shall not be touched here.

Looking back to the multi-director theory of Sec. 5, we recall that this concept is completely identical with 3D continuum mechanics for parameter expansions $l, m, n \to \infty$. Based on our solid shell assumption of linear displacements over the sublayer thickness h_L, all displacement contributions in (9)

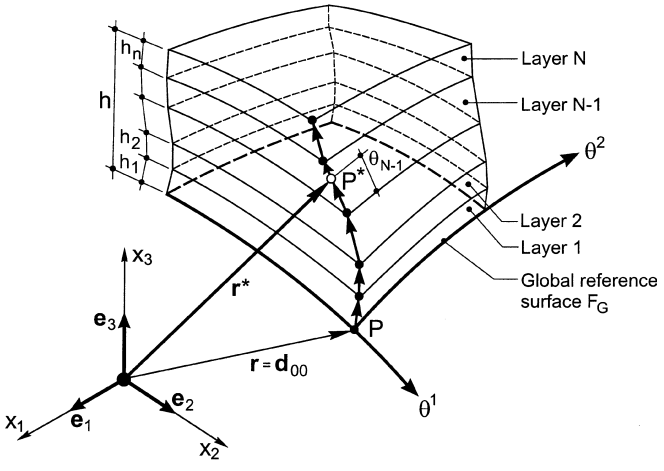

Fig. 10. Coupling of a package of solid shell elements in their nodal points

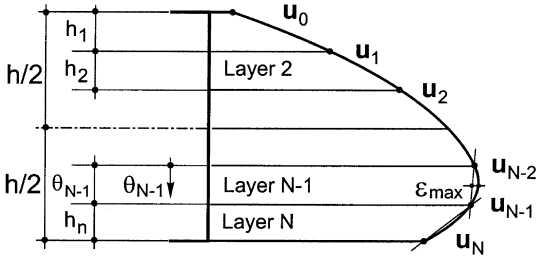

Linear displacement interpolation layer N-1:

$$\bar{\mathbf{u}}_{N-1}(\theta_{N-1}) = \mathbf{u}_{N-2} + (\mathbf{u}_{N-1} - \mathbf{u}_{N-2}) \frac{\theta_{N-1}}{h_{N-1}}$$

Maximum interpolation error:

$$\varepsilon_{\max N-1} = /\!/\, \mathbf{u}_{N-1}(h_{N-1}/2) - \bar{\mathbf{u}}_{N-1}(h_{N-1}/2) /\!/$$

$$\approx (\mathbf{u}_{N-1,\theta\theta}(h_{N-1}/2) \cdot \frac{1}{2} \cdot (\frac{h_{N-1}}{2})^2$$

Fig. 11. Polygon interpolation of displacements over thickness of the package

$$\mathbf{u}^* = \sum_{n=0,1}^{\infty} \theta^n \mathbf{u}_n \ , \tag{108}$$

which are formed by the open space of polynomials θ^n, will be approximated by a polygon of N (straight) vectors over h. Figure 11 illustrates this linear interpolation, demonstrating that constant and linear displacement constituents over each individual layer thickness h_L as over the total thickness h will be reproduced exactly. Higher-order displacement contributions will be approximated. Figure 11 adds an estimate of the maximum interpolation error $\varepsilon_{\max}$, derived from a Taylor series expansion of (108).

Assuming, for comparison, all single displacement contributions $\mathbf{u}_n$ of the polynomial terms θ^n of same order of magnitude, we derive from Fig. 11 the relative error bound of this concept

$$\varepsilon_{\max} = \frac{n(n-1)}{2N^2} \ . \tag{109}$$

For our solid shell package of Fig. 10, we can expect for each polynomial displacement contribution a rate of convergence of $1/N^2$ towards the unknown 3D solution. For higher polynomial contributions, the rate of convergence slows down because of the increasing numerator in (109).

Let us explain the typical solution's behavior by the example of the thin square plate on Fig. 12, [12], a problem with extreme Poisson locking effects. Here, we have compared the results computed with shell models of different numbers of layers, with and without EAS-supplement. All models are based on the eight-noded trilinear, isoparametric solid shell element, [23, 33]. The plate structure is simply supported along all edges and uniformly loaded by p^3. All dimensions and stiffness parameters are given in Fig. 12.

The results of different evaluations of the central deflection are plotted in Fig. 12 against the number of elements per (half-) edge. The analytical solution $w = 21.29324$ is assumed to be 'exact', and gained from the classical double series approach. Obviously, the single-layer element with EAS-supplement approximates this value even for a 4x4 discretization (21.27521) with high accuracy, while the same element without EAS-supplement converges to a completely wrong value (17.38826). For the 8x8 discretization, the solutions for 2, 3 and 4 layers, all without EAS-supplement, overcome their locking tendency and obviously converge for $N \to \infty$ towards the analytical value.

As we have explained, the transversal strain enhancement $\tilde{\varepsilon}_{33}$ of the EAS-concept on Fig. 8, linear along h, is a first step into a second-order approximation, towards 3D 'truth'. In a layered approach of solid shell elements without EAS-supplement, such behavior can only be approximated in step-wise manner because of constant strains ε_{33} along h. Similar behavior with respect to other locking defects was found in many computed examples, [6, 23, 33]. To generalize this experience, layered approaches will converge to the 3D solution also without ANS- or EAS-supplements, provided a sufficiently refined mesh and $N \to \infty$. However, the use of

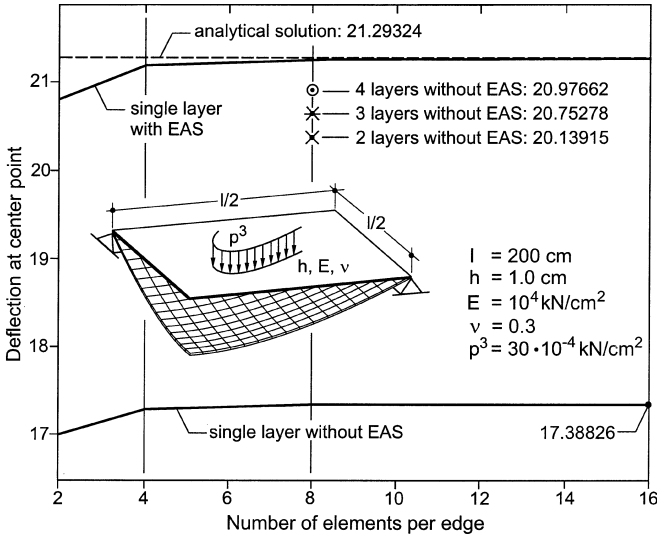

Fig. 12. Square plate: central point deflection due to different shell models

these two techniques is recommended; after all, they play the role of effective convergence accelerators.

11 Conclusions

The most general concept for systematic derivation of shell-like approximations of 3D continua are multi-director theories, gained by integral transformations of the 3D origin in the thickness direction θ^3. Classical shell theories turn out to be augmented linear approximations of such multi-director models, solid shell concepts form complete linear approximations. Both approaches approximate mechanical 3-dimensionality only by the zeroth (resultants) and first-order moments, with the consequences of considerable modeling errors and convergence problems. Multi-layer shell models are capable to approach 3-dimensionality much better, they are asymptotically correct at $N \to \infty$, clearly for the price of higher computational effort. For sufficient number of layers, (stiffness-dependent) locking defects are weakened. However, locking remedies such as ANS- or EAS-concepts are still recommended for use in the single layers, then interpreted as convergence accelerators.

References

1. **Actis, R.L.; Szabó, B.A.; Schwab, C.:** Hierarchic models for laminated plates and shells. Comput Methods Appl Mech Eng 172(1) (1999) 79–107
2. **Ahmad, S.; Irons, B.M.; Zienkiewicz, O.C.:** Analysis of thick and thin shell structures by curved finite elements. Int J Numer Methods Eng 2 (1970) 419–451
3. **Armero, F.:** On the locking and stability of finite elements in finite deformation plain strain problems. Comput Struct 75 (2000) 261–290
4. **Babuška, I.:** The p and h-p versions of the finite element method: The state of the art. In: Voigt, R.G.; Dwoyer, D.L.; Hussaini, H.Y. (eds.) Finite Elements, Theory and Applications, pp. 199–239 Springer-Verlag 1988
5. **Başar, Y.; Ding, Y.; Schultz, R.:** Refined shear-deformation models for composite laminates with finite rotations. Int J Solids Struct 30 (1993) 2611–2638
6. **Başar, Y.; Hanskötter, U.; Jun, D.:** Error-controlled nonlinear simulation of shell structures. In: CD-ROM Proc of the Fourth Int Coll on Computation of Shell & Spatial Structures (IASS-IACM 2000).
7. **Başar, Y.; Krätzig, W.B.:** Theory of shell structures. Series 18: Mechanik/Bruchmechanik. Fortschritts-Berichte VDI. Düsseldorf, VDI Verlag 2001
8. **Başar, Y.; Weichert, D.:** Nonlinear continuum mechanics of solids. Berlin, Springer 2000
9. **Betsch, P.; Stein, E.:** An assumed strain approach avoiding artificial thickness straining for a non-linear 4-node shell element. Commun Numer Methods Eng 11 (1995) 899–909
10. **Bischoff, M.; Ramm, E.:** Shear deformable shell elements for large strains and rotations. Int J Numer Methods Eng 40 (1997) 4427–4449
11. **Bischoff, M.; Ramm, E.:** On the physical significance of higher order kinematic and static variables in a three-dimensional shell formulation. Int J Solids Struct 37 (2000) 6933–6960
12. **Bockhold, J.:** Assumed-Strain-Konzepte für kontinuumsbasierte, dreidimensionale Schalenformulierungen. Diploma Thesis, Institute for Statics and Dynamics, Ruhr University Bochum 2001
13. **Büchter, N.; Ramm, E.:** Shell theory versus degeneration - a comparison in large rotation finite element analysis. Int J Numer Methods Eng 34 (1992) 39–59
14. **Budiansky, B.; Sanders, J.L.:** On the 'best' first-order linear shell theory. In: Progress in Appl Mech the Prager Anniversary Volume, pp. 129–140. New York Macmillan 1963
15. **Düster, A.; Bröker, H.; Rank, E.** The p-version of the finite element method for three-dimensional curved thin walled structures. Int J Numer Methods Eng 52 (2000) 673–703
16. **Dvorkin, E.N.; Bathe, K.-J.:** A continuum mechanics based four-node shell element for general non-linear analysis. Eng Comput 1 (1984) 77–88
17. **Green, A.E.; Laws, N.; Naghdi, P.M.:** Rods plates and shells. Proc Camb Phil Soc 64 (1968) 895–913
18. **Green, A.E.; Naghdi, P.M.:** Non-isothermal theory of rods, plates and shells. Int J Solids Struct 6 (1970) 209–244
19. **Green, A.E.; Zerna, W.:** Theoretical elasticity. Oxford, Clarendon Press 1968/1954
20. **Hauptmann, R.; Doll, S.; Harnau, M.; Schweizerhof, K.:** 'Solid shell' elements with linear and quadratic shape functions. Composite Struct 79 (2001) 1671–1686
21. **Hauptmann, R.; Schweizerhof, K.:** A systematic development of solid-shell element formulations for linear and nonlinear analyses employing only displacement degrees of freedom. Int J Numer Methods Eng 42 (1998) 47–70
22. **Jun, D.:** Adaptive Strategien für nichtlineare Finite-Element-Simulationen von Schalentragwerken. PhD Thesis, Institute for Statics and Dynamics, Ruhr University Bochum, 2002
23. **Jun, D.; Hanskötter, U.; Krätzig, W.B.:** Adaptive strategies for the nonlinear simulation of shell structures. In: CD-ROM Proc of European Congress on Comput Meth in Appl Sci and Eng (ECCOMAS 2000)
24. **Kienzler, R.:** Eine Erweiterung der klassischen Schalentheorie, der Einfluß von Dickenverzerrungen und Querschnittsverwölbungen. Arch Appl Mech 52 (1982) 311–322

25. Klinkel, S.: Theorie und Numerik eines Volumen-Schalen-Elementes bei finiten elastischen und plastischen Verzerrungen. PhD Thesis, Institute for Structural Mechanics, University of Karlsruhe, 2000
26. Klinkel, S.; Gruttmann, F.; Wagner, W.: A continuum based three-dimensional shell element for laminated shell structures. Comput Struct 71 (1999) 43–62
27. Koiter, W.T.: A consistent first approximation in the general theory of thin elastic shells. In: Proc of IUTAM-Symposium on the Theory of Thin Shells, pp. 12–33. Delft-Amsterdam, North-Holland 1959
28. Koiter, W.T.: A systematic simplification of the general equations in the linear theory of thin shells. Proc Koninkl Nederl Akad Wetenschappen, Series B 64 (1961) 612–619
29. Krätzig, W.B.: Allgemeine Schalentheorie beliebiger Werkstoffe und Verformungen. Ingenieur-Archiv 40 (1971) 311–326
30. Krätzig, W.B.: Optimale Schalengrundgleichungen und deren Leistungsfähigkeit. Z Angew Math Mech 54 (1974) 265–278
31. Krätzig, W.B.: On the structure of consistent linear shell theories. In: Koiter, W.T.; Mikhailov, G.K. (eds.) Theory of Shells, pp. 353–368. Amsterdam: North-Holland Publ. Comp., 1980
32. Krätzig, W.B.: 'Best' transverse shearing and stretching shell theory for nonlinear finite element simulations. Comput Methods Appl Mech Eng 103 (1993) 135–160
33. Krätzig, W.B.; Jun, D.: Multi-layer multi-director concepts for *d*-adaptivity in shell theory. Comput Struct 80 (2002) 9–10, 719–734
34. MacNeal, R.: A simple quadrilateral shell element. Comput Struct 8 (1978) 175–183
35. Naghdi, P.M.: The theory of shells and plates. In: Flügge, S. (ed.) Handbuch der Physik VI, pp. 425–640 Berlin, Springer 1972
36. Noor, A.K.; Burton, W.S.; Peters, J.M.: Assessment of computational models for multilayered composite cylinders. Int J Solids Struct 27 (1991) 1269–1286
37. Pagano, N.J.: Exact solutions for composite laminates in cylindrical bending. J Composite Mat 3 (1969) 398–411
38. Pandya, B.N.; Kant, T.: Higher-order shear deformable theories for flexure of sandwich plates. Int J Solids Struct 24 (1988) 1267–1286
39. Parisch, H.: A continuum-based shell theory for non-linear applications. Int J Numer Methods Eng 38 (1995) 1855–1883
40. Phan, N.D.; Reddy, J.N.: Analysis of laminated composite plates using a higher-order shear deformation theory. Int J Numer Methods Eng 21 (1985) 2201–2219
41. Ramm, E.: Geometrisch nichtlineare Elastostatik und finite Elemente, 1976. Habilitationsschrift, Bericht Nr. 76-2, Institute of Structural Mechanics, University of Stuttgart.
42. Reddy, J.N.: A simple high-order theory for laminated composite plates. J Appl Mech 51 (1984) 745–752
43. Reddy, J.N.: On refined computational models of composite laminates. Int J Numer Methods Eng 27 (1989) 361–382
44. Schoop, H.: Oberflächenorientierte Schalentheorien endlicher Verschiebungen. Arch Appl Mech 56 (1986) 427–437
45. Simo, J.C.; Fox, D.D.: On a stress resultant geometrically exact shell model I: Formulation and optimal parametrization. Comput Methods Appl Mech Eng 72 (1989) 267–304
46. Simo, J.C.; Fox, D.D.; Rifai, M.S.: On a stress resultant geometrically exact shell model II: The linear theory; computational aspects. Comput Methods Appl Mech Eng 73 (1989) 53–92
47. Simo, J.C.; Fox, D.D.; Rifai, M.S.: On a stress resultant geometrically exact shell model III: Computational aspects of the nonlinear theory. Comput Methods Appl Mech Eng 79 (1990) 21–70
48. Simo, J.C.; Rifai, M.S.: A class of mixed assumed strain methods and the method of incompatible modes. Int J Numer Methods Eng 29 (1990) 1595–1638
49. Truesdell, C.; Noll, W.: The non-linear field theories of mechanics. In: Flügge, S. (ed), Handbuch der Physik III/3, pp. 1–602 Berlin, Springer 1965
50. Zastrau, B.; Schlebusch, R.; Matheas, J.: Surface-related shell theories for the treatment of composites and contact problems. In: CD-ROM Proc of Fourth International Colloquium on Computation of Shell & Spatial Structures (IASS-IACM 2000)
51. Zerna, W.: Mathematisch strenge Theorie elastischer Schalen. Z Angew Math Mech 42 (1962) 333–341